Finite Element Analysis (FEA) of a Ramjet Structure

a project presented to
The Faculty of the Department of Aerospace Engineering
San José State University

in partial fulfillment of the requirements for the degree
Master of Science in Aerospace Engineering

by

Sofie Tafolla

August 2022

approved by
Dr. Maria Chierichetti
Faculty Advisor

ABSTRACT

Finite Element Analysis (FEA) of a Ramjet structure

The overall project objective is to use a Finite Element Analysis (FEA) on a ramjet structure to analyze and validate the design's performance as it reaches Mach 3 at an altitude of 8 km. First, a MATLAB code will be made to determine the outcome of what altitude and velocity can realistically be reached. Once determined, the forces acting on the vehicle at Mach 3 at an altitude of 8km will be determined using a numerical aerodynamic model through Missile Datcom and are then applied to a finite element model of the ramjet developed in ANSYS To determine the maximum stresses on the structure.

ACKNOWLEDGMENTS

I would like to express my deepest gratitude to all of those who have supported me during this time. More specifically, to my advisor, Dr. Maria Chierichetti for her invaluable guidance, patience, and expertise. In addition, I would also like to give special thanks to all of my professors at San Jose State University for their all of their support throughout graduate career. Last but not least, I would like to express my appreciation to my family and friends for their unwavering encouragement and support throughout the years.

Table of Contents

Deleted: i
Deleted: ii
Deleted: 15
Deleted: 15
Deleted: 17
Deleted: 20
Deleted: 28
Deleted: 30
Deleted: 32

List of Figures

Deleted: .

Deleted: .

List of Tables

Deleted: .

Deleted: .

Nomenclature

Symbol	Definition	Units
P	Pressure	*Pa*
P_0	Initial Pressure	*Pa*
P_e	Engine Exhaust pressure	*Pa*
P_3	Burner Pressure	*Pa*
V	Velocity	*m/s*
L	Length	*m*
d	Diameter	*m*
$\dot{m}$	mass flow rate	*kg/s*
m_0	Initial mass flow rate	*kg/s*
M	Mach	*N/A*
M	Mass Matrix	*N/A*
K	Stiffness Matrix	*N/A*
M_0	Initial Mach	*N/A*
T	Temperature	*K*
T_0	Initial Temperature	*K*
T_3	Temperature upon re-entry	*K*
t	Time	*s*
I	Axial Impulse function	*N/A*
S	Entropy	*J/K*
h_f	Enthalpy	*N/A*
R	Specific Gas Constant	*N/A*
A	Area	M^2
η_e	Exhaust Efficiency	*N/A*
η_b	Burner Efficiency	*N/A*
η_c	Combustion Efficiency	*N/A*
γ_c	Specific heat of the combustion chamber	*N/A*
γ_e	Specific heat of the Exhaust	*N/A*
γ_0	Specific heat of the freestream	*N/A*
ψ	Principal determinant of thermodynamic cycle efficiency	*N/A*
S_{ref}	Reference Area	m^2
C_D	Coefficient of drag	*N/A*
C_f	Coefficient of friction	*N/A*
C_{pb}	Coefficient of pressure of the burner	*N/A*
q_∞	Fluid Density	kg/m^3
ω_i	Natural Frequency	*Hz*
$\frac{V_{fx}}{V_3}$	Ratio of fuel injection with respect to the axial velocity	*N/A*
M	Mass Matrix	*N/A*

Abbreviations

FEA	Finite Element Analysis
CFD	Computational Fluid Dynamics
CEA	Chemical Equilibrium Analysis
CAD	Computer Aided Model
km	Kilometers
M	Meters
NASA	National Aeronautics and Space Administration
DTK	Defense Technical Information Center
AIAA	American Institute of Aeronautics and Astronautics
VLOAD	Vehicle Loads program

Chapter 1. Introduction

1.1 Motivation

The motivation for this study is to perform ramjet structural analyses using Finite Element Analysis (FEA) using SolidWorks and ANSYS to analyze, optimize, and validate design performance parameters at Mach 3 and an altitude of 8 kilometers. Modeling the engine performance, fuel efficiency, mass properties, and structural loading will provide comparative design validations for ramjet engines, with the outcome being an optimized ramjet engine for high-speed, high-altitude flight conditions.

1.1.1. Introduction

Over the years, interest in the technological improvements in propulsion has been exponentially growing because of the mounting pressure to reach higher speeds and altitude capabilities. This desire to fly higher and faster has given many engineers the incentive to push the limits of what was currently possible. An example of a notable engineer who did this was Otto Lilienthal, who pushed the limits of what was possible for gliders in the late 1890s, repeatedly breaking world records for his time up to his death in 1896 [11]. His knowledge and tutelage impacted many engineers, most notably the Wright brothers. According to authors Markus Raffel et al., the Wright brothers were able to study past technological developments, such as what Otto Lilienthal had done, to achieve their first powered flight in 1903 [19]. This became the catalyst for the ramjet, and since then, many improvements and advances have been made to Wright's original four-cylinder horizontal engine, with automatic inlet valves [1]. This engine, credited with being the first controlled, powered, heavier-than-air flight on 17 December 1903, allowed the glider to reach up to 7 miles per hour (mph), which reached a distance of 36 meters for 12 seconds [7]. During the early 1900s, this was an incredible accomplishment that paved the way for innovative new propulsion system designs that could surpass the thrust and efficiency of the Wright Brother's engine. These designs include improvements to internal combustion engines, turboprop, ramjet, scramjet, and electric propulsion systems. More specifically, the ramjet engine was designed to surpass all previous records of the original Wright brothers' engine. It is an airbreathing propulsion system that generates thrust depending on the mass flow through the engine, while the Wright brother's engine was dependent on gasoline that fed into the shallow chamber mixed with air. The heat from the crankshaft vaporized the mixture causing it to pass through the intake manifold into the cylinders. From there, ignition was accomplished by opening and closing two contact breaker points in the combustion chamber, thus generating thrust [1].

For comparison, as described by authors Krisna, et al., "...the top speed of a commercial airliner powered by a turbofan engine can be up to 1.2 Mach, whereas the top speed for a ramjet aircraft is about 6-7 Mach..." [11, p.1]. At speeds as high as Mach 6-7, the ramjet structure experiences several forces that impact the structural integrity of the aircraft. A ramjet engine can also cruise up to 30 km in altitude, experiencing forces that impact the vehicle's structure, such as drag, thrust, and overall weight. The structural integrity of the ramjet will have to endure the forces acting on it. This paper will discuss the methodologies necessary to determine the structural integrity of a ramjet vehicle when experiencing forces at high speeds and altitudes. To prevent the structural integrity of the aircraft from failing, simulated tests must be completed

before physical testing. These precautions include running a Finite Element Analysis (FEA) on the structure of the ramjet to ensure that the forces experienced at Mach 6-7 and the altitude needed would be able to keep the structural integrity of the aircraft.

1.2. Literature Review

1.2.1 Background

The ramjet is an airbreathing propulsion system that uses the vehicle's forward motion and incoming airflow to generate thrust. It uses a thermodynamic process to manipulate the state variables, such as temperature, pressure, and volumes in gas to generate work that can be used to produce thrust. In the early 1900s, many engineers aimed to solve a common problem in propulsion, including solving the weight to thrust challenges that internal combustion engines typically had. Two engineers, Kronach Lorin and Greggory Lake, investigated propulsion systems that did not have streamwise obstructions, which at the time were called ejector ramjets [5]. In 1909, Lake received a patent for the first treatises for the design of a subsonic ramjet. In 1913, Lorin published the second treatise. In 1917 and 1920, French engineers Ernest MoRize and Henry F. Merlot advanced these concepts with the first ejector ramjet concept and began testing in France during the 1915s. Improvements were made to Lorin's and Lake's initial design that increased the amount of static thrust originally produced [6]. Progress continued with engineer Ben Carter when he patented the first practical ramjet structure to enhance artillery shells in 1926. As described by author Ronald S. Fry, this structure had "considerable insight for the time and employed a normal shock inlet with either a conical nose/annular or central cylindrical duct," which is what is used to this day [7, p. 32]. A year later, in 1927, Albert Fono of Hungary patented the first conical-nosed Liquid Fuel Ramjet (LFRJ). The LFRJ design incorporated what is typically seen in modern ramjet engines, such as a converging-diverging diffuser, flame-holders, combustor, and a converging-diverging nozzle [6].

The Talos program, led by Wilbur H. Goss of the Applied Physics Laboratory (APL) in 1945, paved the way for the future of supersonic flight. This program encompassed the first "supersonic, radar-guided, ramjet-propelled missile, launched by a solid-propellant booster rocket and carrying a payload of about 600 pounds of explosive." [14, p.1]. The Talos ramjet missile had a total of 750 successful flights, which inspired the supersonic VANDAL target vehicle to launch 320 missiles with a success record of 98% during its operation from 1980 till the early 2000s [16]. Adapting to the challenges that Talos faced, engineers over the next century developed improvements in technologies such as Computational Fluid Dynamics (CFD) codes as well as code analysis and validation methodologies, air induction technologies, propulsion/airframe and integrations, and combustion technologies that used improved design tools and techniques such as fuel mapping and heat transfer distributions [11]. These improvements impacted the vehicle's performance, specific examples of these improvements were done to the vehicle's aerodynamics, combustor design, thermochemical and engine performance modelling and many more [5]. This research and initial design ultimately laid the foundation for the design of the scramjet engine, which is capable of flight at higher altitudes and speeds than the ramjet.

Typically, ramjets are used for both aircraft and missile applications because of their numerous advantages, which include the ability to attain speeds up to and above Mach 5, a reduced overall aircraft weight because of the smaller engine, its lighter and more

straightforward design than standard turbine-based engines, and their ability to withstand higher operational temperatures [10]. Because of these advantages, ramjet engines are used in numerous missile applications ranging from air-to-air, air-to-surface, surface-to-air, and anti-ship applications. They are also used in numerous aircraft applications, with the most notable being its use with the SR-71 Blackbird. Developed in the 1960s and operated into the late 1990s, the SR-71 was a supersonic reconnaissance aircraft powered by a hybrid engine composed of a ramjet and turbojet engine. More specifically, after the United States developed a small reconnaissance vehicle named the D-21, the SR-71 was used to assist the vehicle in launching and was powered by an engine that resembled the Bomarc RJ-43-MA JP-7-fueled LFRJ engine. It successfully reached speeds above Mach 3, achieved altitudes of 92,000 ft, and covered over 3,000 miles in range [20]. All variations of the ramjet design helped shape the design of modern engine technologies.

The ramjet is composed of three main components: the diffuser, the combustion chamber, and the converging-diverging nozzle. The diffuser takes the incoming supersonic airflow and compresses the air to increase the static pressure and temperature of the air while maintaining constant stagnation pressure throughout the cycle [10]. The thermodynamic cycle that the ramjet experiences are detailed by the Brayton cycle, which consists of four processes, as seen in Figure 1.

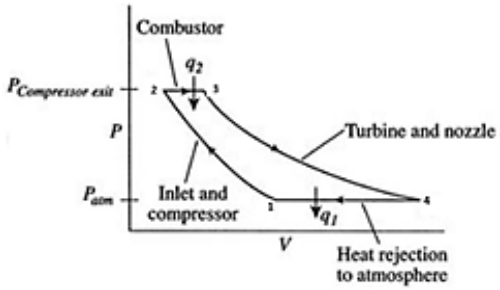

Figure 1. Brayton cycle [6]

States 1 to 2 represents an isentropic compression in the inlet to the compressor. States 2 to 3 to maintain constant pressure with heat addition because the combustion area is considered an open area after the compressor where the fuel is sprayed into. The fuel begins to burn to generate thermal energy; this action increases static temperature from states 2 to 3, but the pressure remains constant because the pressure will equilibrate throughout the chamber. States 3 to 4 show isentropic expansion, during which its enthalpy is transformed into kinetic energy. The compressor uses the work done during this state, while the remaining work accelerates the fluid for jet propulsion. Lastly, during states 4 to 1, the fluid is cooled to its initial condition at constant pressure, assuming this is an ideal ramjet with no pressure loss [6]. However, because of the assumption that this is an ideal ramjet, according to the author of Elements of Gas Turbine Propulsion, Jack Mattingly, the following assumptions are made:

1. There is no loss in thermal or kinetic energy.

2. The pressure in the inlet and the exhaust sections is equal to the back pressure.

3. The total pressure does not change during heating.

4. The working fluid is an ideal gas in which the specific heat is constant.

These assumptions are used to benefit the flow and to increase the mass flow rate for the combustor. The static fluid pressure entering the combustor's entrance will reduce the ramjet's dynamic air pressure. It also uses energy generated by shockwaves, such as the ones generated by the wedge seen just in front of the combustor, which is used to generate normal shocks just after the fuel injections, as shown in Figure 2.

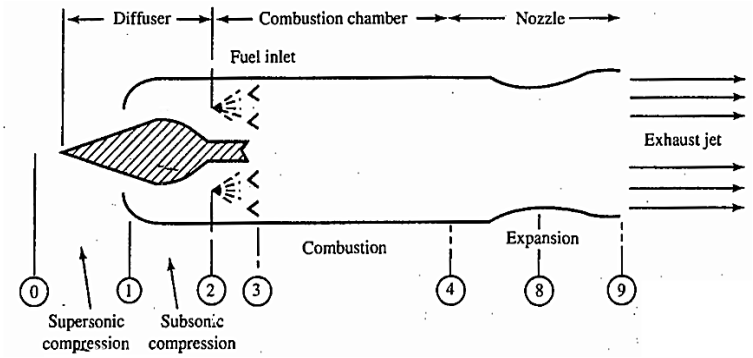

Figure 2. Flow through a ramjet engine [7]

These shockwaves are created when the initial wave moves faster than the local speed of the air. A disturbance carries the energy through the medium and generates a shock. A series of consecutive shocks are called shockwaves which carry the combined energy of all the shocks propagating through the medium [6]. Because the flow is supersonic, the diffuser captures the shockwaves and generates a low-pressure region with no shockwave effect formed at the inlet. However, this region is small and surrounded by a high-pressure region. Because of this pressure difference, the diffuser generates an automatic compression area with the help of shockwaves. The pressure difference, in turn, reduces the flow speed within the combustion chamber, helping the combustion efficiency by providing sufficient time for the fuel to diffuse with the working fluid. As the shock travels through the duct, it will produce a reflected wave proportional to the velocity and pressure fluctuation. When the frequency of these fluctuations is low enough, the shocks will respond in a " … quasi-steady fashion due to rapid change in flow properties" [5]. This indicates that at every moment in time, the shock affects the flow. The structural formation of the duct results in an additional shockwave while the fuel is being injected, and a second wave is generated that assists the mixing process. In addition, the high pressure and temperature air travel into the combustion chamber, where fuel is injected into the chamber, increases the airflow temperature in the chamber and thus increases the fluid velocity and thrust. Due to the shockwave's temperature increase, the shock-induced combustion reaction time decreases [6].

Lastly, the airflow travels into the last component of the ramjet, the converging-diverging nozzle; because of the nozzle's geometry, its pressure decreases, and the fluid air accelerates once more to reach higher velocities. However, this reaction depends on the relative pressure experienced by the nozzle, specifically if the pressure drops across the nozzle. For example, if

the pressure drop experienced is less than critical, the velocity experienced through the nozzle will be less than the speed of sound; however, if the pressure drop across the nozzle is more than critical, then the exhaust from the nozzle will be faster than the speed of sound [6].

The flow through the nozzle is accompanied by a partial dissipation of kinetic energy and heat losses through the structure's walls, and this is joined by the flow's stagnation pressure decreasing and entropy increasing. Understanding how the ramjet engine functions are crucial to understanding what the loads could be on the vehicle and its performance. Once the vehicle's performance can be measured, other tools, such as NASA's VLOAD program, can determine the loads the vehicle will be experiencing during flight.

1.2.2. Finite Element Analysis

An integral part of any product's design cycle is validating its design to react to real-world conditions before manufacturing begins. In this study, a Finite Element Analysis (FEA) is performed to investigate the potential design issues seen in the model when undergoing various testing conditions, particularly those experienced by a ramjet reaching speeds up to Mach 6 and thousands of km in altitude. The basic approach that FEA uses is the division of the physical domain or the model into smaller pieces of finite elements, with the partial differential equations used to represent the physics of the model to simplify and capture the system's behaviour at each of the elements. The equations are then collected together to capture the system's behaviour as a whole under various initial conditions. FEA is utilized in various engineering fields due to its versatility and many advantages, such as having no geometric restrictions, no limitation in boundary conditions or loading situations, and its capability to handle complex restraints and analyze models composed of non-homogenous materials. With these advantages in mind, FEA is used to investigate numerous aerospace applications before costly prototypes are made. Specific examples include the transportation of solid rocket motors (SRMs) as described by authors Qu and Zhang, who discovered that "the propellant grain of the SRM could result in cracking and dewetting in these storage conditions. These significant problems are induced by the stress and strain in the SRM propellant, which is undetectable by current nondestructive inspection methods. It is important to simulate the stress and strain in the SRM propellant because it confirms the critical area and assists in evaluating the damage of the motor" [18, p.1]. Alternatively, authors Schwane and Xia established a finite element model of a rocket engine nozzle to generate the loads generated by the combustion process. In this study, FEA will be used to understand the vehicle's performance at a certain altitude and conditions using an FEA program called ANSYS Mechanical. Using ANSYS Mechanical, static structural analysis will be done using the loads obtained from a semi-empirical aerodynamics code design tool called Missile DatCom.

The loads for this simulation were obtained through a code by the United States Air Force called Missile DatCom. The program was developed to provide the user with an aerodynamic design tool for preliminary designs, more specifically, to estimate the aerodynamics of different missile configuration designs. Because the program uses axisymmetric or elliptically shaped body configurations, it can be assumed to be interchangeable with the elliptical body used for the ramjet body configuration.

1.3. Project Proposal

The overall project objective is to utilize Finite Element Analysis (FEA) on a ramjet structure to analyze, optimize, and validate the design's performance as it reaches Mach 3 at an altitude of 8 kilometres. ANSYS will then be used to perform the FEA using these expected flight conditions. Once the analysis is done, its feedback will be used to optimize the ramjet's structure, and the FEA process will be repeated on the new ramjet's structure to ensure that it is structurally sound. The following are detailed objectives for MATLAB, SolidWorks and ANSYS.

1.3.1. MATLAB Objective

- Model the ideal ramjet using MATLAB
    - Ideal ramjet includes the following stages:
        - inlet
        - compressor
        - combustion chamber
        - exhaust
    - Code will focus on the engine performance:
        - More specifically, the results of the parameters will determine the outcome of what altitude and velocity can be reached. This will have a major impact on the kind of forces the structure can be experienced.
        - The forces experienced at specific altitudes and speeds will greatly depend on the aforementioned equations.

1.3.2. SolidWorks and ANSYS objectives

- Modeling the ideal ramjet using SolidWorks and ANSYS;
    - A computer-aided design (CAD) model will be made through SolidWorks for initial testing; when the model has been completed, ANSYS will then be used to compute the FEA. This process will then be repeated once the new changes have been made to the preliminary design of the ramjet to ensure its structural integrity.
    - 5 different mesh size elements were done to perform a grid generation comparison.
    - A modal and static structural analysis will be done and results compared to one another.
        - Static structural analysis will use the loads obtain by Missle Datcom .
        - Pressures experienced on the vehicle will be applied as a variable load.

1.3.3. Results

- The results obtained through ANSYS mechanical for a modal and static structural analysis will be analyzed with the ramjet structure.
- Future possible work and challenges faced

1.4. Methodology

This analysis will include deriving the forces that the ramjet structure would experience at that altitude and speed. A code to properly size the ramjet for its operational requirements will be

generated, which may derive the amount of thrust and fuel needed for flight and determine the material needed for the given conditions.

This report's first step is collecting numerous benchmarks to prove that the methodology implemented is correct. Initially, a MATLAB script will be generated and determine the different values, such as stagnation temperature and pressure throughout the ramjet, such as the compressor, nozzle, combustion chamber, and the overall engine performance. It is assumed that this is an ideal ramjet, with relevant formulas and relationships obtained from *Hypersonic Airbreathing Propulsion* by William H. Heiser when developing the MATLAB script. Once completed, a computer-aided design (CAD) model will be created using SolidWorks for initial testing. When the model has been completed, ANSYS will then be used to compute the FEA. In addition to this process, a program called Missile DatCom will be used to generate pressure distributions at an altitude of 8km. The information from Missile DatCom will then be used and imported into ANSYS as a variable load applied to the model. This process will then be repeated once the new changes have been made to the preliminary design of the ramjet to ensure its structural integrity.

Chapter 2. Development of an Ideal Ramjet Model

Understanding the engine performance is crucial to improving a preliminary design of a ramjet engine. A parametric cycle analysis determines the engine performance at different flight conditions and design limitations. The overall goal of completing a parametric cycle analysis is to relate the engine's performance parameters to the design limitations of the flight environment to determine the component design characteristics that best complete the mission's objectives. To perform the overall analysis, a MATLAB script was generated using an ideal ramjet model, which includes the inlet, compressor, combustion chamber, and exhaust section. These components will be used to determine the overall engine performance of the ramjet to determine the results of what altitude and velocity are physically possible with the initially given parameters. These initial parameters will significantly impact the kind and magnitude of forces the physical structure will be experiencing when in flight. The forces will significantly vary based on the equations formulated by Heiser, later described in section 2.2 [9].

2.1. Modeling Assumptions

Several assumptions are considered in developing an initial simplified model of a ramjet. The first two assumptions are that the working fluid passing through the engine must be in its equilibrium state at all times and that the combustion process is replaced without the addition of heat, mass or the process of changing the chemical ingredients of air [1]. The second assumption is that the cycle must return to its original state, which is called the Brayton cycle, which is accomplished through 4 processes that show the absolute static temperature and specific entropy diagram, seen earlier in Figure 1. These assumptions ensure that the system's entropy does not change and that the system is ideal.

Additional assumptions, as mentioned by Mattingly [12] include:

- There will have to be an isentropic compression and expansion process in the diffuser, compressor, and the nozzle.
- Constant pressure must be kept in the combustion chamber and the fuel rate must be less than the airflow through the combustor such that:
  - $\frac{m_f}{m_c} \ll 1 \; and \; m_c + \; m_f = 1$
- Air must be flowing through the engine and must behave as a perfect gas with constant specific heats.
- The engine exhaust pressure must be equal to that of the ambient pressure $P_e = \; P_0$
- The working medium must experience a series of equilibrium processes that will return to its original state, this will be accomplished by the Brayton Cycle.

These additional assumptions are needed to simplify the thermodynamic cycle when analyzing the engine's combustion, compression, and expansion process.

To understand how a ramjet functions, the Brayton cycle is used to understand the thermodynamic process throughout the engine as the fluid flows through the inlet, compressor, combustion chamber, and exhaust sections. The cycle is explained in the following passage and is crucial to performing the engine performance analysis, which can be seen in Figure 1.

Adiabatic compression occurs from points 0 to 3, with its freestream temperature and static temperature at the burner's entry. As the static temperature increases, and due to the loss of

energy caused by skin friction and shock waves travelling through the engine, the entropy increases from its original value to its new value at the entry of the burner. Typically these losses are not negligible. However, because the system is ideal or isentropic, the losses are negated, and there is no change in entropy.

The next step in the Brayton cycle is from points 3 to 4, as seen in Figure 1. As the flow travels through the combustion chamber, it will have a constant static pressure but have an increase in static temperature going from T_3 to T_4 without the addition of mass to the system. As described by Mattingly [1], there are numerous reasons why static pressure through the combustion chamber was chosen to be held constant rather than other flow parameters such as Mach number or flowthrough area. The first is that by keeping the static pressure constant, the flow avoids the possibility of boundary layer separation. If the boundary layer were to separate, this would induce an additional drag force as a result of the pressure difference within the combustion chamber [1]. The second is that it is desirable for the combustion chamber to be designed to withstand the peak pressure within the chamber.

The flow then enters points 4 to 10 as seen in Figure 1 and travels through the combustion chamber to the end of the nozzle. During this process the ramjet will experience an adiabatic expansion, causing the burner's static pressure to be $P_3 = P_4$ and the pressure experienced at the nozzle to equal freestream static pressure $P_{10} = P_0$. Similar to the process preceding this section, the losses experienced by skin friction and shockwaves cause the entropy to increase from the burner's exit value of S_4 to S_{10} at the end of the adiabatic expansion process. But again, because we consider the process ideal, none of these losses are considered. Lastly, as the thermodynamic cycle closes, the process returns to its original temperature -entropy state, which consists of points 10 to 0. This drives the conclusion that the velocity of the air is constant, or in other words, the velocity of the remaining air at the end of the cycle is identical to the thrust produced at the end of the adiabatic expansion process. This last step completes the Brayton cycle and returns the cycle to its original state. Depending on the parameters used, the cycle may have different solutions.

Each parameter will impact the engine analysis differently; the first crucial parameter is the Thermodynamic cycle efficiency, which can be used for numerous applications. One of the most notable is that the results of the thermodynamic cycle efficiency can show that the static temperature at the beginning of the combustion chamber cannot indefinitely increase, that there is a limit that prevents dissociation in the exhaust flow. In short, the burner exit and entry static temperatures will begin to increase, this will cause the loss in energy to unequilibrated dissociation will begin to dissolve the benefits that are usually associated with having a higher thermodynamic efficiency. However, the temperature experienced in the engine does have a limit and is dependent on several variables such as the flight altitude, Mach number, inlet and outlet energy losses, fuel type, fuel to air ratio, and the burner and exhaust geometry. Because dissociation and reassociation are gas kinetic phenomena the limit is best stated in terms of static temperature at the beginning of the combustion chamber [1]. However, because the working fluid is air and the design's fuel to air ratio is often near or at stoichiometric value and because of this assumption the maximum allowable compression temperature T_3 can be assumed. As described by Heiser [8], the maximum allowable temperature of T_3 is almost always between the range 1440-1670K. Because the assumption that the air is calorically perfect and is assumed to be a calorically perfect gas dissociation effects are negligible and is assumed to have a constant ratio of specific heat $Y_c = 1.36$. As previously stated, since there is a limit to the allowable

compression temperature T_3, there is also a restriction on the burner entry Mach number M_3. This relation is seen in the following equations:

$$T_t = T_0\left(1 + \frac{\gamma_c - 1}{2} {M_0}^2\right) = T_3\left(1 + \frac{\gamma_c - 1}{2} {M_3}^2\right) \tag{2.1}$$

Equation (2-1) can be rewritten to show the relation with the burner Mach number:

$$M_3 = \sqrt{\frac{2}{\gamma_c - 1}\left\{\frac{T_0}{T_3}\left(1 + \frac{\gamma_c - 1}{2} {M_0}^2\right) - 1\right\}} \tag{2.2}$$

In addition to these equations, the following equations will be used after dividing the ramjet engine into three different components. Before beginning the analysis, the ramjet engine shall be divided into three sections, which will be compression, combustion and expansion sections, for simplicity, as seen in Figure 2 [3].

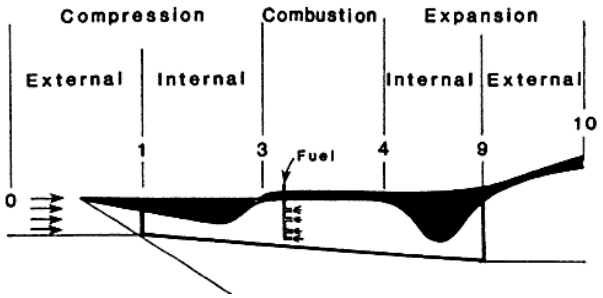

Figure 3. Geometry of a ramjet engine [1]

Starting with the compression section of the ramjet engine. the first variable that will be used in the analysis is the Stream Thrust function:

$$S_{a0} = \frac{I}{m} = V_0\left(1 + \frac{RT_0}{{V_0}^2}\right) \tag{2.3}$$

With I being the Axial Impulse function, γ = 1.4, and m being the mass flow rate:

$$I = pA(1 + \gamma M^2) \tag{2.4}$$

Additionally, V_0 represents the initial velocity, R is the specific gas constant (R= 287) and T_0 represents the freestream temperature. Continuing with the steps recommended by Heisen, the following equation is used to find the maximum allowable compression temperature:

$$T_3 = \psi T_0 \tag{2.5}$$

Under the condition that ψ follow the restriction:

$$\psi = \frac{T_3}{T_0} \geq 1 \tag{2.6}$$

Or equation (2-6) can be written in terms of efficiencies for the combustion chamber η_c, exhaust η_e, burner η_b :

$$\psi = \sqrt{\frac{\eta_c \eta_e}{1-\eta_c \eta_e} * \frac{\eta_b f h_{br}}{T_0 C_{p0}}} \tag{2.7}$$

With ψ being the principal determinant of thermodynamic cycle efficiency that can directly be used to impose a limit on the allowable temperature in the compression section. The velocity of the flow at the entrance of the combustion chamber can be described by equation (2.8):

$$V_3 = \sqrt{{V_0}^2 - 2C_{pc}T_0(\psi - 1)} \tag{2.8}$$

With C_{pc} being the specific heat at constant pressure, furthermore the adiabatic pressure ratio between the pressure of the combustion chamber compared to the freestream pressure that originates from the following equation (also known as the adiabatic compression process):

$$\frac{P_3}{P_0} = \left\{\frac{\psi}{\psi(1-\eta_c)+\eta_c}\right\}^{\frac{C_{pc}}{R}} \tag{2.9}$$

Lastly, the ratio between the area of the combustor with respect to the freestream is also examined with the below equation:

$$\frac{A_3}{A_0} = \psi \frac{P_0}{P_3} * \frac{V_0}{V_3} \tag{2.10}$$

With all of the preceding equations, an analysis of the compression section is complete. The combustion portion of the three components of the ramjet follows the analysis. Two solutions must be explored with the compression section to ensure all possible design possibilities for the ramjet. These two solutions consist of constant pressure and a constant area combustion section. For simplicity, the four following quantities can be assigned for the following values, considering the system to be ideal for both possible designs.

The first of which is $\frac{V_{fx}}{V_3}$ which represents the ratio of fuel injection with respect to the axial velocity to V_3, $\frac{V_f}{V_3}$ which represents the ratio of the fuel injection with respect to the total velocity to V_3. Then the terms $C_f * \frac{A_w}{A_3}$ represents the burner effect drag coefficient. Then the absolute static enthalpy h being represented by the following equation:

$$h = C_{pb}(T - T^o) \tag{2.11}$$

Lastly, the absolute sensible enthalpy of fuel entering the combustor is represented by the term h_f.

Onto the first possible solution, with the assumption that the ramjet is utilizing a Constant Pressure Combustion, the first equation to be used in this process is the velocity at the entrance of the combustion chamber:

$$V_4 = V_3 \left\{\frac{1 + f * \frac{V_{fx}}{V_3}}{1+f} - \frac{C_f * \frac{A_w}{A_3}}{2(1+f)}\right\} \tag{2.12}$$

Then using the conservation of energy equation to solve for the temperature at the combustion chamber:

$$T_4 = \frac{T_3}{1+f}\left\{1 + \frac{1}{C_{pb}T_3}\left[\eta_b f h_{br} + f h_f + f C_{pb} T^o + (1 + f * \frac{{V_f}^2}{{V_3}^2})\frac{{V_3}^2}{2}\right]\right\} - \frac{{V_4}^2}{2C_{pb}} \quad (2.13)$$

And lastly, the area ration between the combustion chamber and the burner:

$$\frac{A_4}{A_3} = (1+f)\frac{T_4}{T_3} * \frac{V_3}{V_4} \quad (2.14)$$

The next possible solution is assuming that the ramjet uses a design that utilizes a constant area combustion section, similar to the process used for a design that uses constant pressure combustion; the velocity at the entrance of the combustion chamber is needed. The equation for the velocity can be determined by utilizing the conservation of momentum and energy equation to form the following:

$$V_4 = \frac{-b \pm \sqrt{b^2 - 4ac}}{2a} \quad (2.15)$$

Where the following equation represents the values used for a, b, and c:

$$a = 1 - \frac{R}{2C_{pb}} \quad (2.16)$$

$$b = \frac{V_3}{1+f}\left\{\left(1 + \frac{RT_3}{{V_3}^2}\right) + f * \frac{V_{fx}}{V_3} - \frac{C_f}{2} * \frac{A_w}{A_3}\right\} \quad (2.17)$$

$$c = \frac{RT_3}{1+f}\left\{1 + \frac{1}{C_{pb}T_3}\left[\eta_b f h_{pr} + f h_f + f C_{pb} T^o + (1 + f * \frac{{V_f}^2}{{V_3}^2})\frac{{V_3}^2}{2}\right]\right\} \quad (2.18)$$

Similar to the ramjet with constant pressure, the temperature at the entrance of the combustor is needed and can be derived by using the conservation of momentum and energy equation to form the following equation:

$$T_4 = \frac{c}{R} - \frac{{V_4}^2}{2C_{pb}} \quad (2.19)$$

Additionally, the pressure ratio between the pressure experienced at the combustion chamber and that of the freestream pressure can be determined by deriving the equation from the conservation of mass equation and using the equation below:

$$\frac{P_4}{P_0} = (1+f)\frac{p_3}{p_0} * \frac{T_4}{T_3} * \frac{V_3}{V_4} \quad (2.20)$$

For both design possibilities, both will use the following equation to determine the Stream thrust function at the entrance of the combustion chamber:

$$S_{a4} = V_4\left(1 + \frac{RT_4}{{V_4}^2}\right) \quad (2.21)$$

Both solutions will have different outcomes, but can be used depending on the design restrictions the designer sets. Once completed, the user may move on to the next portion of the analysis, which is an analysis of the expansion component from points 4 to 10, in which the flow travels from the combustion chamber to the exhaust. Similar to the steps used in the preceding sections, the temperature at the exhaust is initially needed:

Using the adiabatic expansion process:

$$T_{10} = T_4\left\{1 - \eta_e\left[1 - \left(\frac{p_{10}}{p_o} * \frac{p_0}{p_4}\right)^{\frac{R}{C_{pe}}}\right]\right\} \quad (2.22)$$

Then using the conservation of energy equation, the velocity at the exhaust can be solved using the following equation:

$$V_{10} = \sqrt{{V_4}^2 + 2C_{pe}\,(T_4 - T_{10})} \quad (2.23)$$

The stream thrust function of the exhaust can be derived using the stream thrust function used in the previous sections:

$$S_{a10} = V_{10}\left(1 + \frac{RT_{10}}{{V_{10}}^2}\right) \quad (2.24)$$

And lastly, using the conservation of mass equation for the area ratio of the exhaust and the inlet is solved using:

$$\frac{A_{10}}{A_0} = (1 + f)\frac{P_0}{P_{10}} * \frac{T_{10}}{T_0} * \frac{V_0}{V_{10}} \quad (2.25)$$

The results of these equations depend on the values used for the parameters that appear in the equations (2.1:25). An endless combination of parameters can be used and will vary the results significantly. The nominal values of free stream thrust analysis calculations are shown in Table 1. Using these values and the preceding equations, various pressures, temperatures, velocities, and specific impulses at various stations of the engine can be calculated. The values seen in table 1. specifically come from an example used in reference [1]. This example was used to test the accuracy of the values generated with different parameters.

Table 1. Nominal case values [1]

Parameter	Value
Freestream (γ_0)	1.4
Combustion Chamber (γ_c)	1.362
Exhaust (γ_e)	1.238
Burner (γ_b)	1.23
Principle determinate of thermodynamic cycle efficiency (ψ)	7.0
Specific heat constant at the Exhaust (C_{pe})	$1510\,J/kgK$
Specific heat constant at the Burner (C_{pb})	$1510\,J/kgK$
Efficiencies at the Burner (η_b), $Combustion\ (\eta_c)\ and\ the\ Exhaust\ (\eta_e)$	.90
Burner effect drag coefficient ($C_f * \frac{A_w}{A_3}$)	.1
Ratio of fuel injection with respect to the axial velocity to V_3 ($\frac{V_{fx}}{V_3}$)	.1
Ratio of the fuel injection with respect to the total velocity to V_3 ($\frac{V_f}{V_3}$)	.5

Chapter 3. Missile Datcom

3.1 Overview

Missiles Datcom is a stability and control prediction code used by the United States Airforce as a conceptual and preliminary design tool. The program's purpose is to provide an aerodynamic design tool that can predict the aerodynamic stability and control characteristics of a conventional missile configuration. For this study, the geometry of the ramjet is based on a cylindrical body and can be compared to a conventional simple rocket or missile geometry. All three structures previously mentioned can be modelled as a cylindrical beam that is unsupported at both ends.

This design tool depends on the goal the user wants to complete and will significantly impact overall missile design. As stated in the Missile Datcom document "Development Feasibility of Missile Datcom by author Steven R. Vukelich, "…the type of mission influences the choice of components which make up the configuration design. The matrix of configurations that satisfy the mission requirements comprises both mission and design requirements" [5, p.5]. It is recommended that Missile Datcom be used for the conceptual, preliminary and point design of a vehicle to choose between accuracy, efficiency and cost.

The program is designed to address the geometric and flight conditions requirements that come from the mission's goal. It utilizes two databases to perform the analysis; the first is Jane's Weapon Systems, which provides an up-to-date open source analysis of offensive and defensive systems in the United States of America. Moreover, the other is experimental data summaries of the Aeromechanic Survey and Evaluation report by author Matthew M Briggs. These databases assist the program with developing trends seen in current missile designs. Results obtained from this assessment are designed with a fineness ratio, which is the length of the streamlined body to maximum length of the diameter of 10. The data is also tested across a broad Mach spectrum and up to 30 degrees of angle of attack. For this study, the body methodology section was used to compute the aerodynamic characteristics of the vehicle's body. For this section, the databases we "were assembled through extensive literature searches of the Defense Technical Information Center (DTK), the National Aeronautics and Space Administration (NASA) and the McDonnell Douglas Corporation libraries and the archive journals and meeting papers of the American Institute of Aeronautics and Astronautics (AIAA). The reports selected were categorized by subject and screened according to the required range of geometry and flight conditions" [4, p.30]. The aerodynamic characteristics used for this study are the pressures along the body under the conditions seen in table 2.

The conditions used in table 2 were explicitly chosen based on the possible criteria that can be reached with the given geometry. Furthermore, to have a minimum variation of flight conditions, such as controlling the vehicle's speed in the test phase altitude, the flight can theoretically maintain a constant temperature, Mach number and temperature by using the isotropic regions of the atmosphere between 10-20km. Ideally, a constant dynamic pressure path would also be required, and this is due to large structures sustaining very high pressures due to the rapidly increasing Mach numbers.

The vehicle's geometry was designed with specific parameters and goals in mind. For example, one goal in designing the geometry was to find the minimum throat area that can

overtake the shock in the nozzle's divergent portion. The shock will be in a more stable position, and the changes in pressure downstream will not result in an unstart. An unstart occurs when there is a severe reduction of air mass flow rate through the engine, which causes a severe loss in thrust. In addition to the last parameter, the mass flow rate at the inlet of the throat must be equal to the flow rate across the normal shock. Moreover, because of the larger throat area that is needed, the total pressure is needed, such as having a higher free stream Mach number to force the shock through the convergent section. This can also be achieved by having the starting Mach number be larger than the cruise Mach number. The Mach number for the vehicle was chosen based on the range of Mach numbers within the supersonic regime, above the cruise Mach number, and as Mach 3.

Along with these parameters, an altitude of 8km was chosen with the altitude, the corresponding density, temperature, velocity and dynamic viscosity. Lastly, the material's weight and cost were also considered when choosing the altitude that the mission was to fly at. The more the vehicle weighed, the more thrust the ramjet's engine would need to generate, causing the inlet of the ramjet to increase in size, increasing the material needed and the overall cost.

Table 2. Boundary conditions used for Missile Datcom

Boundary Conditions used in Missile Datcom:	
Altitude	8000 km
Temperature	26240 K
Density	0.5256 $\frac{kg}{m^3}$
Pressure	35600 $\frac{N}{m^2}$
Velocity	923.8090 $\frac{m}{s}$
Mach	3
Dynamic Viscosity	1.5406e-5 Pa·s
Reynolds Number	6.00e7

Two altitudes were looked into for this analysis, one at 8km and the other at the maximum altitude of 20km with both reaching a speed of Mach 3. Missile Datcom exports several files of aerodynamic data as seen in figure 4. Moreover, the ANSYS Mechanical program offers several choices on importing different variables when defining tabular loads for this analysis. The external data tool retrieves the altered data files exported from Missile Datcom.

Furthermore, the program's inputs use Fortran Namelist. The namelist themselves are column independent and be input multiple times for the same input case. An example of some of the needed input are the flight conditions, reference quantities, the asymmetrical/elliptical body definition, experimental data, inlet geometry and many more [2]. Each namelist is required to be filled; for example, according to Blake, " This namelist defines the flight conditions to be run for the case. The program is limited to no more than 20 angles of attack and 20 Mach

number/altitude combinations per case at a fixed sideslip angle, aerodynamic roll angle, and panel deflection angle" [2, p.16]. While for the reference quantities, "A vehicle scale factor (SCALE) permits the user to input a geometry that is scaled to the size desired. This scale factor is used as a multiplier to the user-defined geometry inputs; it is not applied to the user input reference quantities (SREF, LREF, LATEEF). If no reference quantities are input, they are computed based upon the scaled geometry. XCG is input relative to the origin of the global coordinate system" [2, p.17]. All of which along with the remaining inputs to calculate the aerodynamic data in the "… 1) Normal force, 2) Axial force, 3) Pitching Moment, 4) Side Force, 5) Yawing Moment, 6) Rolling Moment, and 7) the derivatives of the above concerning angle of attack and sideslip angle." [2, p.95]. However, there are unique options "… of the code such as experimental data substitution and configuration incrementing depending on the methods by which the aerodynamic coefficients are calculated. These options are executed in the subroutine SYNTHS" [2, p.96].

Unit	Name	Usage
2	for002.dat	Namelists for the input "case" are read from unit 8 and written to unit 2 by Subroutine READIN. The namelists for the "case" are read from unit 2.
3	for003.dat	Plot file of aerodynamic data, written at user request (using PLOT card) to unit 3 by Subroutines PLOT3, PLTTRM, or PLTUT9.
4	for004.dat	Common block data, written at user request (using WRITE card) to unit 4 by Subroutine SAVEF.
5	for005.dat	User input file, read from unit 5 by Subroutine CONERR.
6	for006.dat	Program output file, written to unit 6.
7	for007.dat	The FORMAT and WRITE control cards are written to unit 7 by Subroutine CONTRL and read by Subroutine SAVEF
8	for008.dat	User input cards read from unit 5 are written to unit 8 by Subroutine CONERR after they have been checked for errors
9	for009.dat	Body geometry data, written at user request (using PRINT GEOM BODY card) to unit 9 by Subroutines SOSE, VANDYK, or HYPERS.
10	for010.dat	Body pressure coefficient data at angle of attack, written at user request (using PRESSURES card) to unit 10 by Subroutines SOSE, VANDYK, or HYPERS.
11	for011.dat	Fin pressure coefficient data, written at user request (using PRESSURES card) to unit 11 by Subroutine FCAWPF.
12	for012.dat	Body pressure coefficient and local Mach number at zero angle of attack, written at user request (using PRESSURES) card to unit 12 from Subroutine SOSE.

Figure 4. Missile Datcom output

The data file that will be used for the FEA analysis is the file that is labelled for010.dat; this file contains the to get the pressure coefficients. Specifically, the file is broken into sections for each flight condition. The first column is the longitudinal location for the geometry, and the remaining columns are the circumferential locations. The columns are then repeated in the same manner for a wide range of angles of attack, such as 30, 60, 90, and 180 degrees. The pressure coefficients are then used to derive the pressure experienced over the vehicle using the following equation:

The results are then imported into an excel sheet where the following equation is used to determine the pressure at different locations:

$$C_p = \frac{p - p_\infty}{\frac{1}{2} \times q_\infty \times V_\infty^2} \tag{3.2}$$

The equation above represents the of coefficient of pressure in terms of pressure and inertia forces. The equation is rearranged to show the following:

$$p = \frac{1}{2} \times q_\infty \times V_\infty^2 + p_\infty \tag{3.3}$$

Where q_∞ represents the fluid density and p_∞ represents at 8,000 km and at 26240 K. Lastly, V_∞ represents the velocity. As previously mentioned, different attack angles would affect the load distributions' symmetry as well as where the transition point would be for the loads.

Additionally, an example of one of the equations used to calculate the coefficient of drag can be seen in the following equation:

$$\frac{C_D}{C_f} = [1 + 1.5(\frac{d}{L})^{1.5} + 7\left(\frac{d}{L}\right)^{3}]\frac{S_{wet}}{S_{ref}} \quad (3.1)$$

With d representing the diameter of the vehicle, L representing the length, the coefficient of frictions, the reference area, and the reference area that interacts with the working fluid. With the given conditions and general dimension of a ramjet geometry seen in the following section, a data file was extracted to represent the pressure coefficients for the vehicle's circumferential location. This data is then imported into Ansys as tabular data to be applied to the vehicle and described in section 4.4.

Chapter 4. Finite Element Analysis

4.1 Geometry

To perform a finite element analysis (FEA), a model of the ramjet model, loads and boundary conditions must be set and used to test the overall performance of the structure in question. The geometry was designed to model a simple ramjet design that would achieve the overall mission goal; to reach an altitude of 8km at Mach 3. These parameters were chosen because of the possibility of it being achievable based on previous literature reviews and the possibility of manufacturing in the future.

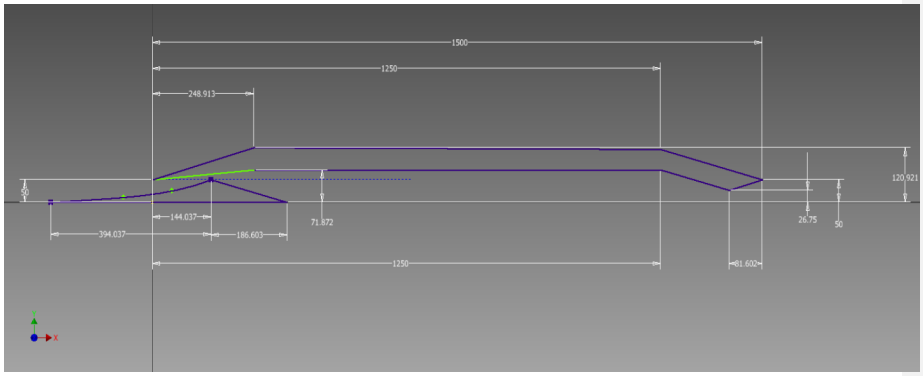

Figure 5. Overall dimensions of the ramjet

The overall length of the body of the ramjet is 1.5m with an inner diameter of .10m and an outer diameter of .0064m. These parameters were chosen based on the internal analysis done for the Vertical Flight Supersonic Test Platform Project, which is being done as a project by the students of San Jose State University. The project is to develop a supersonic/hypersonic flight test platform under specific flight conditions. Overall, the project introduces an additional requirement that the means for achieving the, "…scalable supersonic flight condition is to incorporate a high-speed airbreathing propulsion system such as a ramjet. This requirement widens the educational scope and value over past rocketry activities, but it is a more efficient method for achieving the throttling performance needed and recurring cost objectives" [4,p.5].

As previously mentioned, the vehicle's geometry was designed with specific goals, which included finding the minimum throat area that can overtake the shock in the nozzle's divergent portion and the mass flow rate at the inlet of the throat must be equal to the flow rate across the normal shock. It concluded to impose a fixed diffuser throat area of $d = 7.9$ cm × 7.9 cm. This area is larger than the minimum area chosen for every altitude for the chosen conditions. These calculations were done by other members of the project using a software called OpenRocket. This program allowed the students to design a model rocket and generate plots that compared the internal flow with the maximum results possible for the given internal geometry parameters seen below.

- A_i = 9 cm × 9 cm
- $A_{t,d}$ = 7.9 cm × 7.9 cm
- A_c = 12.5 cm × 12.5 cm
- A_e = 12.5 cm × 12.5 cm
- A_e/A_t = 1.5

An example of these results can be seen in Figure 6 and Figure 7.

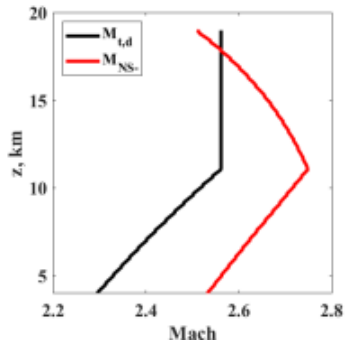

Figure 6. Mach vs altitude [7]

Figure 6. shows a comparison between the allowable Mach number for the throat of the ramjet (black) and the allowable Mach number for the nozzle section (red) to the possible altitude achievable. Moreover, an analysis was done to determine the effects that the possible mass of the ramjet would have on the achievable Mach number and possible altitude, as seen in figure 6.

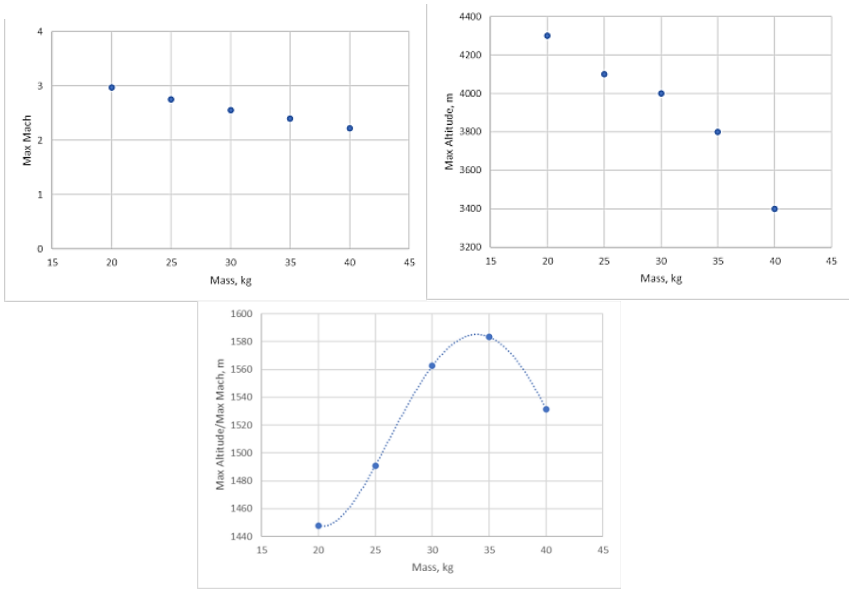

Figure 7. Possible mach number vs mass (left), possible altitude vs mass (right) and altitude/mach number ratio vs mass (bottom) [7]

Using a simple curve fit for the Altitude/Mach number ratio vs the mass allows the user to visualize what are the parameter possible for the desired goal.

The material of the ramjet needs to be versatile so that it may withstand not only the forces it will be experiencing at altitudes of 8 to 20km but also the extreme temperatures at those specific conditions, both internally because of the combustion process the ramjet will perform and externally, from the forces the ramjet will be experiencing. Multiple materials, such as aluminum steel and titanium, all common materials for ramjets engines, were investigated, but AISI 347 Annealed Structural Steel (SS) was chosen due to its tensile and compressive properties yield strength of 2.5e+08Pa.

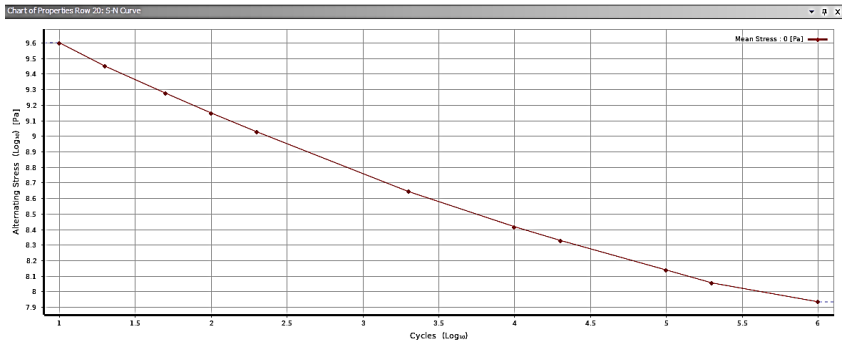

Figure 8. S-N curve provided by ANSYS that shows the alternating stress vs the number of cycles experienced

The material of the vehicle was chosen because of its high value for tensile yield strength and its Tensile ultimate strength.

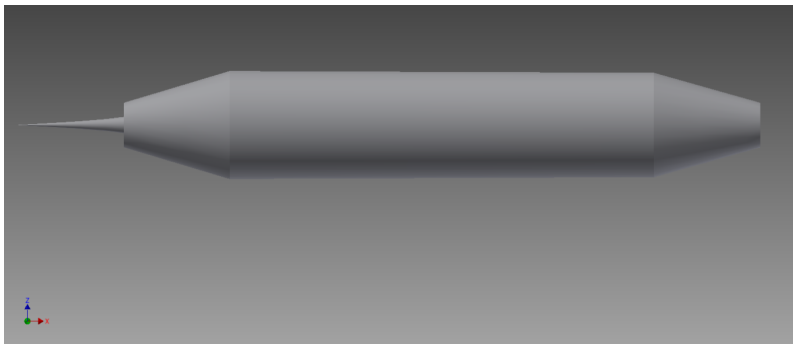

Figure 9. SolidWorks model

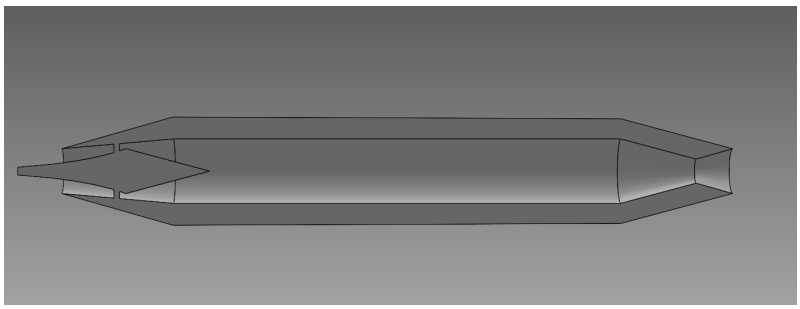

Figure 10. SolidWorks model cross sectional view

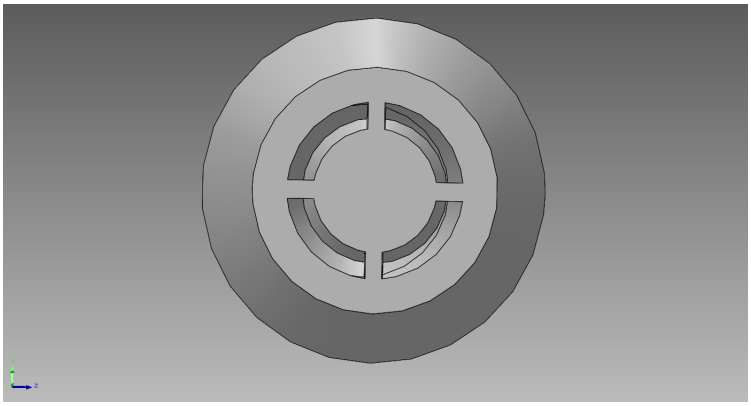

Figure 11. SolidWorks model cross sectional view of the nozzle

Additional parameters included in the modal that can be seen in the geometry is the addition of 4 columns protruding from the inlet spike. The model was simplified due to the complexity of the geometry needed to model a ramjet. The columns were designed to hold the inlet spike in place and to prevent the inlet spike from being free-floating. In addition to adding the columns, a model section along the x-axis was made as a fixed structure to represent how the ramjet would be attached to the rest of the vehicle. This fixed support is essential when generating the analysis results by applying a variable load or performing modal analysis.

4.2 Grid Generation

Before proceeding with the ramjet's modal and static structural analysis, grids will have to be made to perform the analysis. Seven meshes were used for the grid generation study for the static structural analysis, beginning with the coarsest mesh of .0200m to the most refined mesh with an element size of .0025m. ANSYS allows the user to manipulate the mesh to be as refined or coarse as needed in a specific model section. For this analysis, the model was broken into two components, the four columns as one component and the remaining body of the ramjet, including the inlet spike as the other component. Because of the difference in components, the vehicle is considered a multi-body part that will affect the mesh.

Beginning with the latter component, face sizing was used; this mesh option was chosen for its being a surface-level mesh that ensures that the geometry is appropriately resolved. This is considered a Hex dominant mesh that allows the user to determine the shape of the element used for the surface. For the analysis, a tetrahedral mesh was chosen because of the simplicity of the geometry. In addition, using a triangular mesh will generate the grid in less computing time. To keep the grid study consistent throughout the meshes, all other parameters, aside from the element size, were kept constant. This decision was made to ensure that the convergence of the solution was solely based on the element size and not another contributing factor. The factors that were kept constant were the growth rate set to 1.2 while skewness and aspect ratio below 1. In addition, as described by author Andreas Lintermann, a quality mesh require that the cells of the mesh have minimal skewness, minimal changes in the cell's volumes between adjacent cells, suitable aspect ratios, and has a sufficient resolution in specific regions. [16]

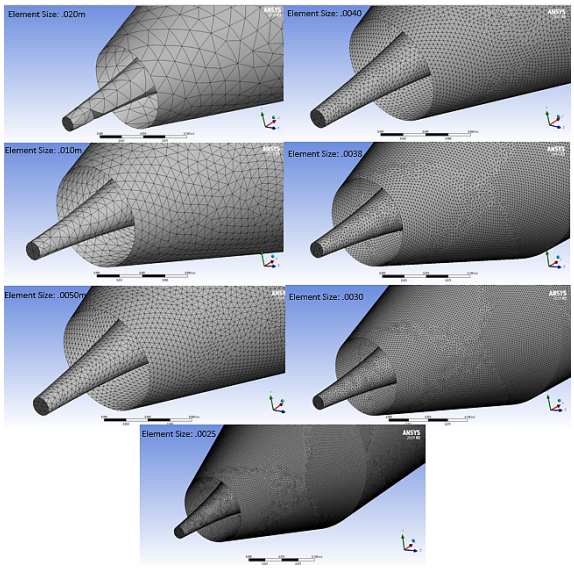

Figure 12. All seven meshes for the static structural analysis

The grid generation study begins with the coarsest mesh that has an element size of .025m; the element size is then halved to be .01m. The mesh is then halved once more to be .005m; following this decrease in element size, the mesh is decreased to .004m to .0035m to .0030m. The grid generation study then ends with the most refined element size of .0025m. The element sizes were chosen initially to be halved of the previous element size, as seen for element sizes .02m,.01m,.005m and .0025m. Because of a lack of processing power and memory for this analysis, the mesh could not be halved from .0025m. For this reason, .004m, .0035m and .003m were chosen to evaluate the ranges between .005m and .0025m. As the refinement of the mesh increase, so does the number of elements and time required to generate the mesh, as seen in table 3.

Table 3. Mesh size comparison between the number element and the time needed to generate the mesh

Mesh size	Number of elements	Time needed to generate
.02m	22,768	6.34s
.01m	101,223	14.81s
.005m	416,635	32.73s
.004m	649,801	2.54 mins
.0035m	728,589	5.11 mins

Mesh size	Number of elements	Time needed to generate
.003m	1,176,346	18.21 mins
.0025m	1,689,354	27.43 mins

Along with the increase in computing time and element size, there was an increased need of computing process needed for each refined run. Nevertheless, these wide range of meshes were chosen to get a large range of meshes to ensure that solution obtained would be grid independent.

4.3 Modal Analysis

A crucial step to understanding a vehicle's structural integrity is determining and understanding the structure's natural frequencies. Typically, modal analysis is a linear analysis that does not require any excitation or load and is solely dependent on the stiffness and mass of the evaluated component. It is essential to check if the natural frequencies coincide with any dynamic loading, which can potentially cause resonance with the excitation force. Excitation forces can lead to excessive vibrations, which can damage the structure. By using a modal analysis to produce mode shapes associated with natural frequencies, the designer can design the vehicle to avoid these specific ranges of frequencies to prevent resonance. In addition, knowing the natural frequencies allows the user to understand better that complex and dynamic behavior is based on the natural frequencies.

To calculate the natural frequencies the linear equation of motion is first used in the following form:

$$\boldsymbol{M}\{\boldsymbol{u}_i\} + \boldsymbol{K}\{\boldsymbol{u}_i\} = 0 \tag{4.2.1}$$

Where **M** represents the mass matrix and K represents the stiffness matrix. By assuming that the component will experience harmonic motion the two vectors can be represented as the following:

$$u_i = \phi_i \sin(\omega_i t + \theta_i) \tag{4.2.2}$$

$$u_i = -w_i^2 \phi_i \sin(\omega_i t + \theta_i) \tag{4.2.3}$$

Substituting equations (4.2.2) and (4.2.3) back into the linear equation of motion (4.2.1) can derive the eigen value problem:

$$\{\{\boldsymbol{K} - \omega_i^2\{\boldsymbol{M}\}\}\ \phi_i = 0 \tag{4.2.4}$$

Where the first portion of the equation represents the natural frequencies with omega ω_i while, the second portion of the equation ϕ_i represents mode shapes.

For this analysis, two different modal analyses were looked into with two different element sizes for the mesh but having the same fixed support. The first had an element size of .01m and produced six natural frequencies and modes:

Table 4. Modes and frequencies for element size .01m

Mode	Frequencies
1	427.05 Hz
2	741.4 Hz
3	728.06 Hz
4	787.66 Hz
5	1192.6 Hz
6	1205.5 Hz

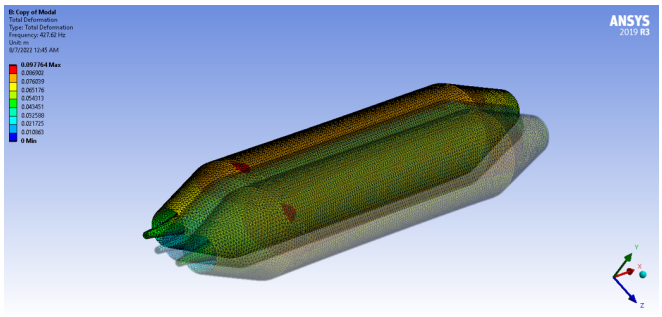

Fig 13. Ansys user interface with an element size of .01m for Mode 1 (rotational).

For the first mode of the analysis with an element size of .01 shows a rotational motion in the z direction, which is continuously repeated. And shows how the model would dynamically respond to excitation.

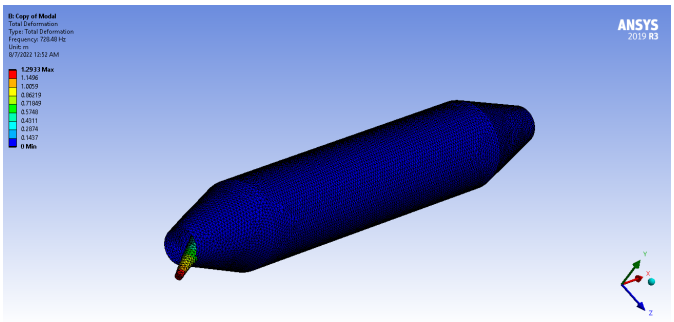

Fig 14. Ansys user interface with an element size of .01m for Mode 2, inlet spike bending.

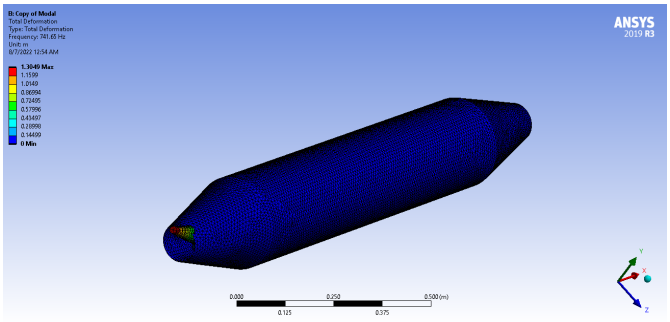

Fig 15. Ansys user interface with an element size of .01m for Mode 3, inlet spike bending.

Figures 10 and 11 both show the inlet spike deforming as a dynamic response to the excitation, figure 10 shows the inlet spike moving vertically in the positive and negative y direction, while in figure 11. The inlet spike is moving horizontally in both the positive and negative z direction.

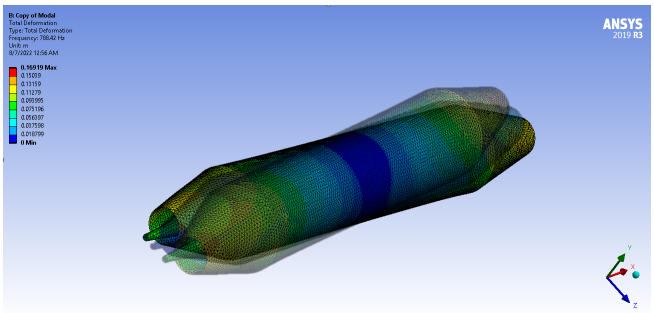

Fig 16. Ansys user interface with an element size of .01m for Mode 4 (rotational).

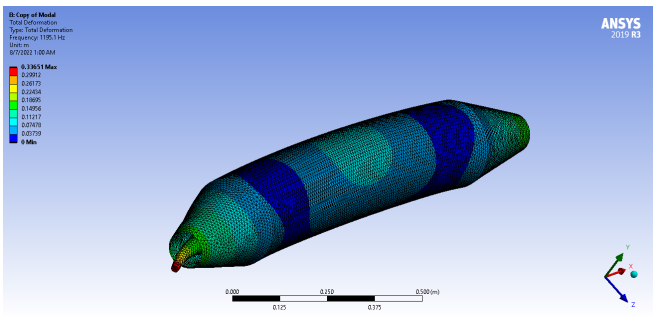

Fig 17. Ansys user interface with an element size of .01m for Mode 5 (bending).

As for Modes 4 and 5, Mode 4 shows the entire vehicle rotating about its center of axis, while Mode 5 has the vehicle along with the inlet spike bending about the center of axis.

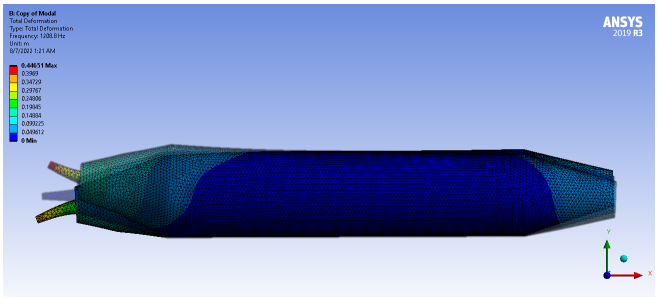

Fig 18. Ansys user interface with an element size of .01m for Mode 6 (bending).

Lastly, there is Mode 6, which shows the vehicle along with the inlet spike bending vertically. Comparing figures (9) and (12), it can be seen how the different natural frequencies affect the total deformation. Using the total deformation information provided by the solution, it can be determined which mode is excited by the forces in a specific direction. For the mesh that uses the element size .01m, the maximum deformation is .09770m for mode 1 and 0.14772m for mode 4. The purpose of these mode shapes is to show how the vehicle's natural frequencies would react to excitation and where the vehicle is prone to experience a high concentration of stress compared to the other regions. Specifically looking at Modes 2,3,5, and 6, it can be determined that the inlet spik would experience the most stress compared to the rest of the vehicle. While the subsequent analysis uses a mesh element size of .0025m, evaluating the same mode shapes:

Table 5. Modes and frequencies for element size .0025m

Mode	Frequencies
1	412.9 Hz
2	664.47 Hz
3	684.47 Hz
4	780.18 Hz
5	1182.5 Hz
6	1185.5 Hz

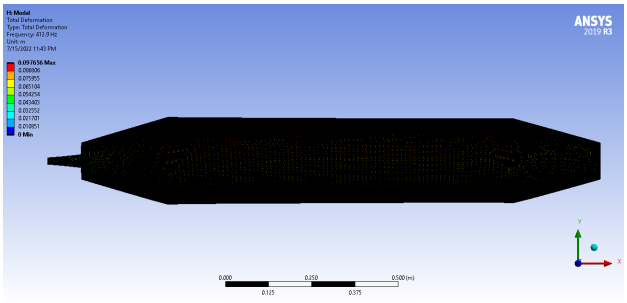

Fig 19. Ansys user interface with an element size of .0025m for Mode 1.

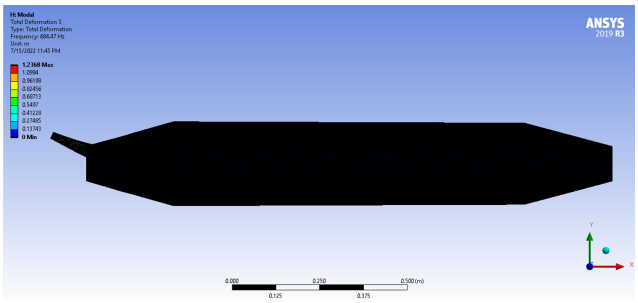

Fig 20. Ansys user interface with an element size of .0025m for Mode 3.

Now comparing figures 15 and 16, it can also be seen how the different natural frequencies affect the total deformation. Similarly, using the solution's total deformation information provided, it can be determined which mode is excited by the forces in a specific direction. The direction in which the deformation occurs is specific to a natural frequency. For example, the deformation seen in figure 16 physically bends the inlet spikes vertically and continues to oscillate in that direction. For the mesh that uses the element size .0025m, the maximum deformation is .097656m for mode 1 and 1.2m for mode 3. Comparing figures 9 and 12 shows an absolute percent difference between modes one is .04%, while the percent difference between modes 3 is 18.84%. The results show that dependent on the frequencies that are being evaluated. The grid refinement can have a significant impact, as seen in the percent difference in mode four or have a minor difference, as seen in mode 1. In the following section, a grid refinement study was done with variable load applied to the whole vehicle.

4.4 Static Structural Analysis

For the second portion of the analysis, a static structural analysis was done to the ramjet vehicle to validate the current geometry configuration. Static structural analysis of the vehicle is assessed by comparing calculated strains in the structure and the material's yield point. If the structure's strains do not exceed the material's yield point with the applied loads, the system suffers only elastic deformations, as seen in the mode shapes, and the structure's shape will be fully restored after the loads are no longer applied. However, if the applied loads exceed the

material's yield point with the applied loads, the shape of the structure will irreversibly deform and possibly cause the structure to fail. This process can be seen in figure 21., once the stress and strain of the material passes the elastic region of the scale, the material begins to deform.

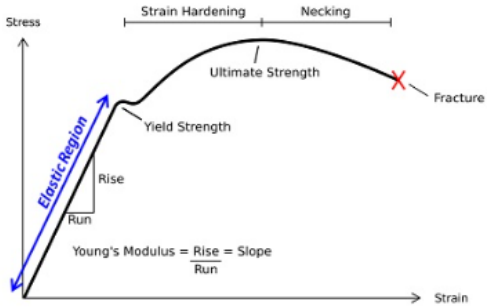

Figure 21. Stress and strain curve [16]

Using ANSYS the analysis can be done to investigate how certain loads, stresses, and strains will react to the vehicle. Similar to the modal analysis, any system can be represented as the following three components in a system:

$$\boldsymbol{M}\{\boldsymbol{u}\} + \boldsymbol{C}\{\boldsymbol{u}\} + \boldsymbol{K}\{\boldsymbol{u}\} = \boldsymbol{F} \tag{4.2.1}$$

Where **M** represents the mass matrix, **C** represents the damping or energy loss experienced by a system, and **K** represents the stiffness matrix. These equations represent a dynamic system. However, for static structural analysis, the inertia and damping terms will be removed and will be left as:

$$\boldsymbol{K}\{\boldsymbol{u}\} = \boldsymbol{F} \tag{4.3.1}$$

Where **K** still represents the stiffness matrix and **F** represents the applied forces. Along with this notation, the forces applied are not time varying and no inertial effects are included. This data is then imported into Ansys as tabular data to be applied to the vehicle.

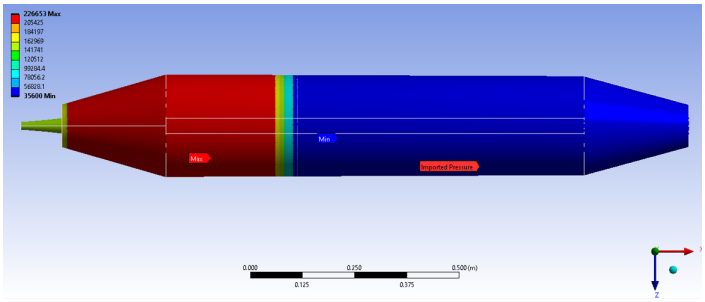

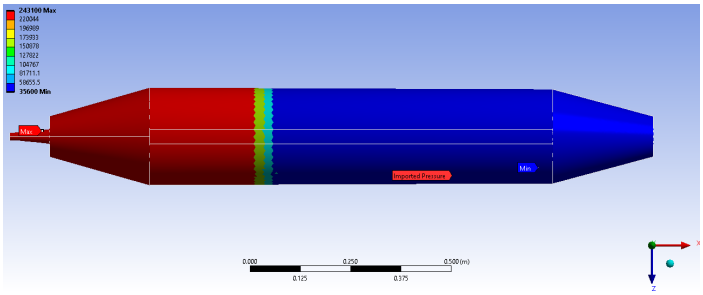

Figure 22. Pressure distributions on the vehicle at 8km (top) and 20km (bottom)

The pressure distributions calculated by Missile Datcom can be seen applied to the vehicle in the following figures. The pressures were applied with a 0 degrees angle of attack for these configurations. And the 0 degrees configuration serves as a baseline for future work. Figure 17 shows the pressure distribution at 8km with a max pressure of 226,653Pa, while the maximum pressure experienced at 20km is 243,100Pa. Figure 18., which shows the pressure distribution at 20km, shows that most of the pressure experience occurs at the front of the vehicle and where the inlet spike is located. Because the angle of attack for the vehicle as it is flying is 0 degrees, the pressure distribution around the vehicle is symmetrical. As the pressure loads travel down the length of the vehicle, the pressures begin to diminish until they reach the minimum pressure.

Chapter 5. Results and Analysis

As previously mentioned, a grid refinement study was done to evaluate the pressure loads calculated from Missile Datcom. The purpose of a grid refinement study is to question and determine the accuracy of the results, more specifically, if the results depend on the grid. If the results depend on the grid, then it is clear that the solution has not truly converged, and the grid will require additional refinement until the results do not change. Having a high-resolution mesh can produce very accurate results. However, the computational time and cost will be high. Versus a coarse mesh can produce an inaccurate result but have a low computational time and cost. A grid refinement study can help the designer determine which grid will help him or she find the most accurate results without having a high computational cost. For this analysis, all of the meshes utilize the same variable load and the same fixed support. The only variation that was done was to the refinement level of the meshes.

The study evaluates the equivalent stress, strain, the force reaction and the total deformation that the vehicle experiences. As expected, the maximum stress the vehicle experienced was the four columns connecting the inlet spike to the rest of the vehicle, as seen in figure 14.

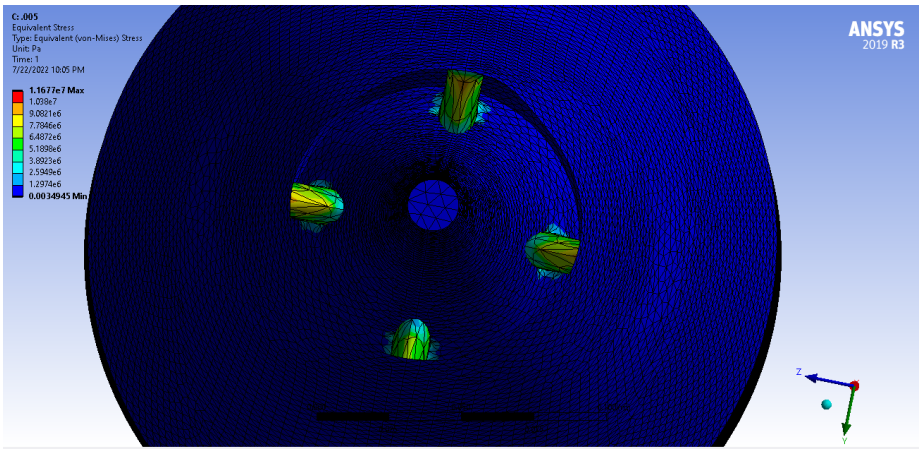

Figure 23. Frontal view of the ramjet with an element size of .005m, maximum stress seen in the four columns

As previously discussed, the four columns were added to the structure to properly connect the inlet spike to the rest of the vehicle. Realistically, the ramjet structure would not include these columns due to the columns causing interference with the flow. However, to simplify this analysis, columns were included to simplify the geometry. The rest of the vehicle is experiencing the minimum value of stress, while the columns experience the maximum amount of stress but are still under the structural steel's tensile yield strength.

Table 6. Description of the mesh refinement study with its respective max stress and percentage difference with the next mesh in order

Element Size	Mesh Number	Max Stress	Percent Difference
0.0200m	1	2.96E+06 Pa	2.85E+02
0.0100m	2	1.14E+07 Pa	1.75E+00
0.0050m	3	1.16E+07 Pa	2.41E+01
0.0040m	4	1.44E+07 Pa	2.71E+01
0.0035m	5	1.83E+07 Pa	7.10E+00
0.0030m	6	1.70E+07 Pa	4.71E+00
0.0025m	7	1.78E+07 Pa	

As seen in table 3. column 3, as the refinement of the mesh increase, the stress experienced to the columns begin to rise until they begin to converge. Column 4 of table 3. shows the percent difference of the initial mesh with the succeeding mesh refinement. As the mesh is refined, the difference in the maximum stress begins to shrink as the mesh becomes more and more refined. Because of these results, the solution for the maximum stress experienced by the vehicle is no longer grid dependent.

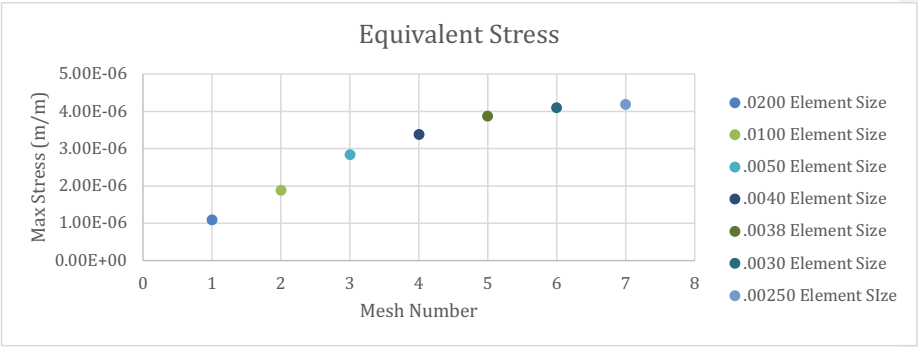

Figure 24. Equivalent stress for all seven meshes

The amount of stress experienced by the vehicle will have an effect on the overall strain. The strain reflects the deformation as a result of the stress experienced. Alternatively, it can be defined as “Strain is essentially the proportional change in the size (length) of the material at a particular point on the object…” [15, P.4].

Table 7. Description of the mesh refinement study with its respective max strain and percentage difference with the next mesh in order

Element Size	Mesh Number	Max Strain	Percent Difference
0.0200m	1	1.10E-06 m/m	7.20E+01
0.0100m	2	1.90E-06 m/m	4.98E+01
0.0050m	3	2.84E-06 m/m	1.93E+01
0.0040m	4	3.39E-06 m/m	1.46E+01
0.0035m	5	3.88E-06 m/m	5.79E+00
0.0030m	6	4.11E-06 m/m	2.01E+00
0.0025m	7	4.19E-06 m/m	

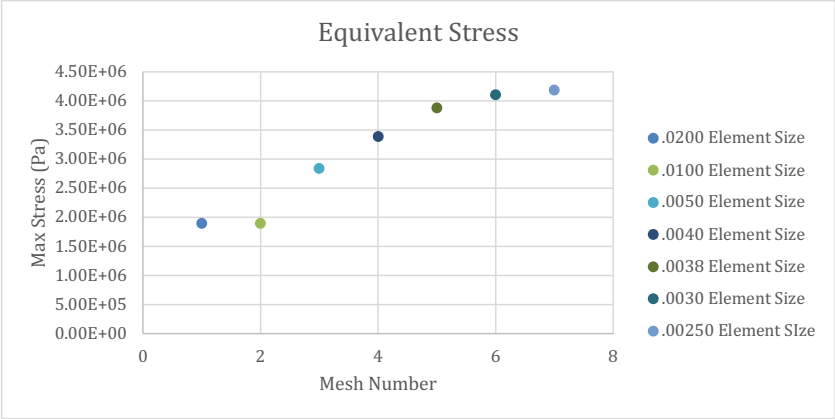

Figure 25. Equivalent stress for all seven meshes

Similarly, the results for the maximum amount of strain that the vehicle is experiencing have a similar trend to what is seen in the maximum amount of stress. As the mesh refinement increases, the difference between solutions becomes smaller and smaller, as seen in table 4. column 4. By looking at figure 16. a trend can be seen as the mesh refinement increase, the trend initially begins linearly, and as the difference in results become smaller and smaller, the trend begins to flatten and converge.

Table 8. Description of the mesh refinement study with its respective max total deformation and percentage difference with the next mesh in order

Element Size	Mesh Number	Total Deformation	Percent Difference
0.0200m	1	2.52E-06m	1.60E+01
0.0100m	2	2.92E-06m	2.87E+00
0.0050m	3	3.01E-06m	2.08E+00
0.0040m	4	3.07E-06m	1.35E+00
0.0035m	5	3.11E-06m	1.10E+00
0.0030m	6	3.14E-06m	4.71E-01
0.0025m	7	3.16E-06m	

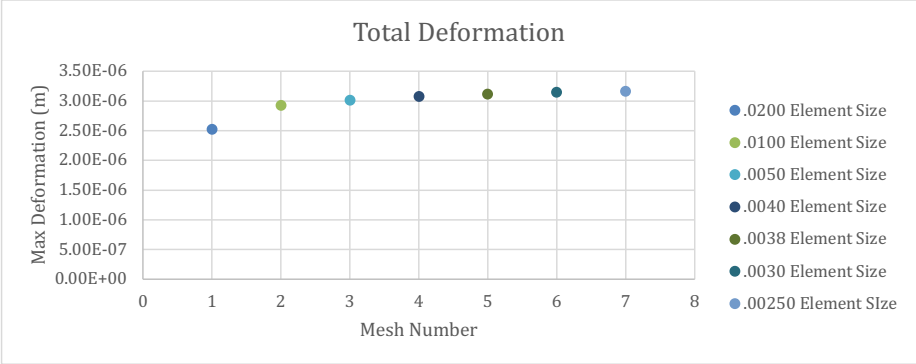

Figure 26. Graph of all seven meshes with respect to their total deformation

Examining the results taken for total deformation, it can be seen that the total deformation is minimal and does not change the structure's shape. In addition, it does not introduce nonlinearity to the system's responses. Investigating figure 17. it can be seen that as the refinement of mesh increases, the solution gradually decreases and converges around a similar solution. However, as expected, the maximum total deformation occurs where the four columns are placed. The deformation occurs because of the forces exerted on the vehicle's body. The columns also resist the forces but still connect the two bodies.

Table 9. Description of the mesh refinement study with its respective max total Force Reaction (X Direction) and percentage difference with the next mesh in order

Element Size	Mesh Number	Force Reaction (X Direction)	Percent Difference
0.0200m	1	6576.7 N	2.49E+00
0.0100m	2	6740.5 N	2.14E+00
0.0050m	3	6596.4 N	6.37E-02
0.0040m	4	6592.2 N	5.76E-02
0.0035m	5	6596 N	1.82E-02
0.0030m	6	6597.2 N	4.55E-03
0.0025m	7	6597.5 N	

Commented [MC1]: units

Commented [MC2]: Add units

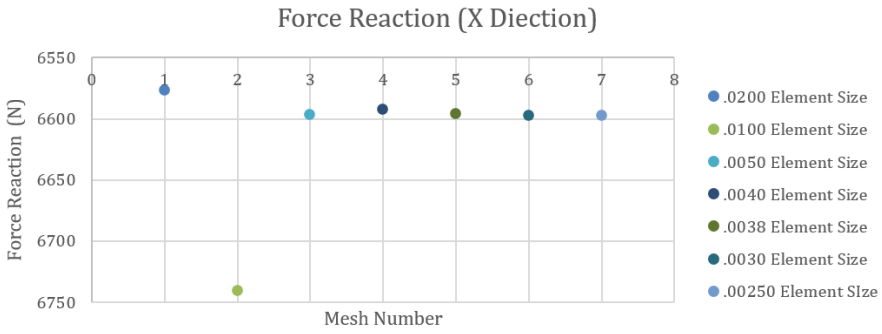

Figure 27. Graph of all seven meshes with respect to their force reaction

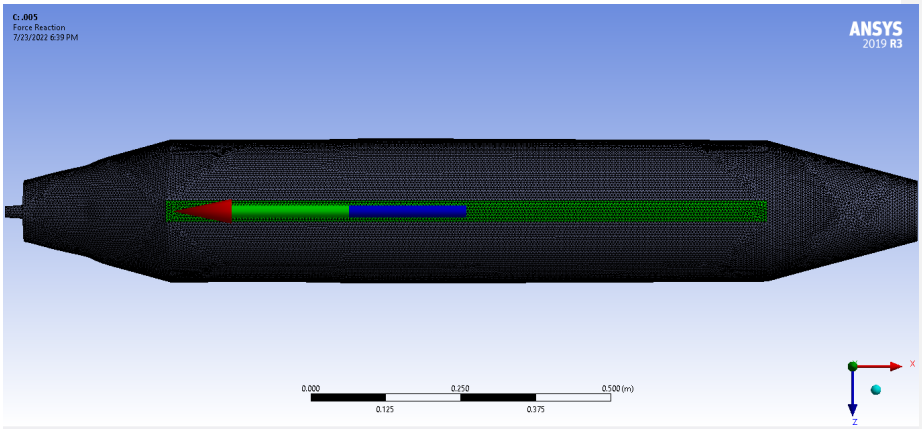

Figure 28. Example of force reaction applied to the model with an element refinement of .005m

The force reaction is used in ANSYS to determine the forces in the x, y, and z directions. More specifically, the forces in the x direction were inspected for this analysis. The force in the x direction proved to be the most significant force of the three directions, followed by the normal forces in the y direction. As the vehicle travels at Mach 3 at 8km, the forces act parallel to the surface, such as the airflow pressure over the vehicle. In column 4 in table 7, the percent difference decreases as the grid resolution increases and converges on a value. These results show that they are not dependent on the grid resolution and are independent.

Table 10. Description of the mesh refinement study with its respective maximum alternating stress and percentage difference with the next mesh in order

Element Size	Mesh Number	Maximum alternating stress	Percent Difference
0.0200m	1	9.90E+05 Pa	9.15E+01
0.0100m	2	1.90E+06 Pa	4.98E+01
0.0050m	3	2.84E+06 Pa	1.93E+01
0.0040m	4	3.39E+06 Pa	1.46E+01
0.0035m	5	3.88E+06 Pa	5.79E+00
0.0030m	6	4.11E+06 Pa	4.10E+01
0.0025m	7	6.79E+06 Pa	

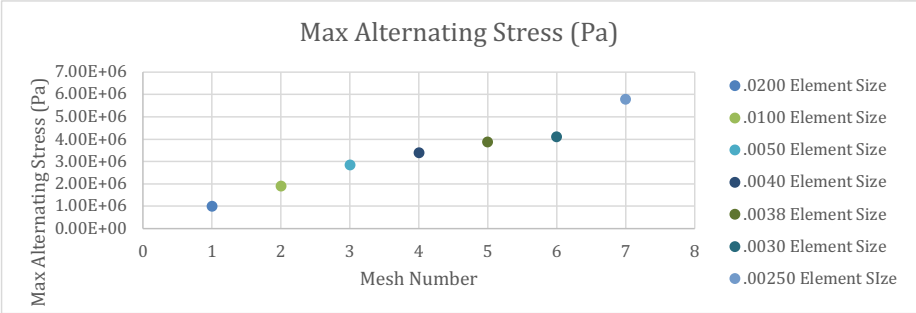

Figure 29. Graph of all seven meshes with respect to their maximum alternating stress

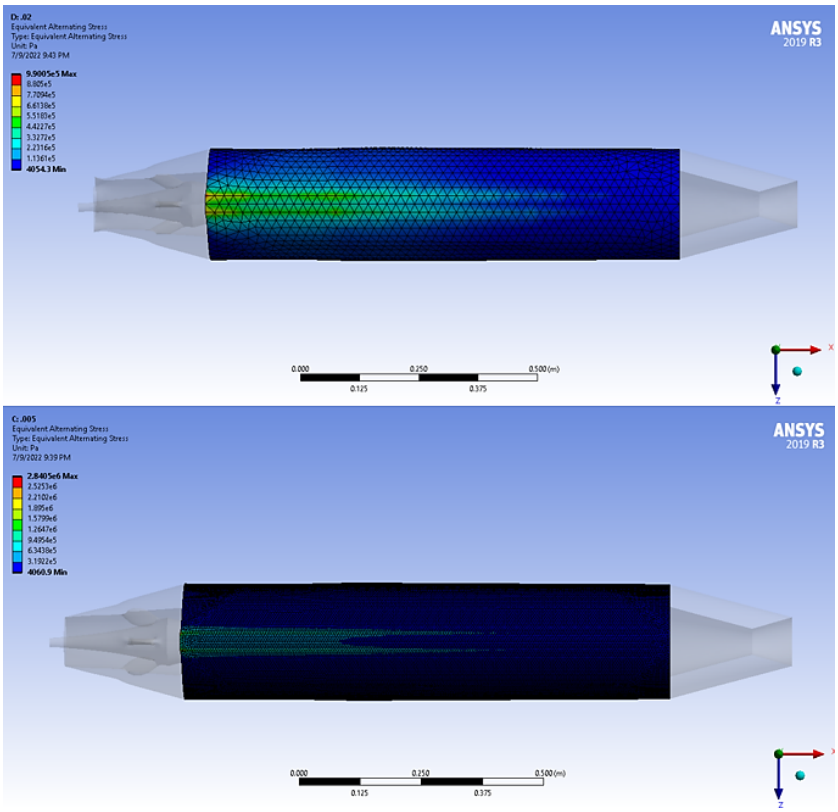

Figure 30. Comparison of alternating stress between a mesh with an element size of .02m (top) and an element size of .005m (bottom)

The maximum alternating stress is inspected between all of the meshes. The equivalent alternating stress analysis can be described by the authors Li, Han, and Duan of Study of Influential Factors of the Vibration Modal of the Rocket Equipment Bay and Structural Improvement Based on Finite Element Analysis as “Thus the “equivalent alternating stress” is the stress used to query the fatigue S-N curve after accounting for fatigue loading type, mean stress effects, multiaxial effects, and any other factors in the fatigue analysis…” [15, P.30]. The stress of the material created by the forces exerted on the body changes in direction and magnitude as time passes. When comparing the grid quality to the overall solution, it can be seen that the resolution of the mesh matters. Investigating figure 30. it can be seen with the coarser grid that there is a more considerable amount of stress over a larger area of the vehicle; however, when the grid is refined, as it is with an element size of .005, the amount of stress over the vehicle is concentrated to only a specific location. Now investigating table 10. as the grid becomes more refined with a minor element size, the stress becomes more concentrated in both located on the vehicle and in value. The finer grid can resolve the maximum alternating stress better than the course grid giving a more accurate result.

Lastly, investigating the results and relating them to the maximum yield stress for chosen material will show that the vehicle is not in danger of failing or experiencing any permanent deformation. With all of the grid generation study, the results show that the vehicle's maximum stress is less than the ultimate yield strength of the material, which is 2.5e+08Pa. In contrast, the maximum stress experienced to the vehicle is located where the four columns conjoin the inlet spike and the rest of the vehicle. The maximum stress experienced is shown when using the most refined mesh of 1.78e+07 Pa, as seen in table 3. Comparing the material ultimate yield strength with the maximum stress will also give the factor of safety. When comparing the two values, the vehicle's safety factor is 13.312. This factor of safety shows that even with the four columns experiencing the highest concentrated stress, the columns would still be above industry standards in terms of safety. As for the rest of vehicle, the factor of safety is substantially higher than the four columns because the rest of the vehicle shows a minimum stress of .00349 Pa. This factor of safety will have to be evaluated for future cases for additional loads. This solution is considered converged because the percent difference gradually decreasing and converging on a value.

Chapter 6. Conclusion and Future Work

This study aims to perform ramjet structural analyses using FEA with SolidWorks and ANSYS to analyze, optimize, and validate design performance parameters at Mach 3 and an altitude of 8 km. This study has shown that the grid refinement study's current model configuration is sufficient to operate at an altitude of 8km and Mach 3. Furthermore, the best grid refinement level for future analysis using this model will have to be the grid that uses the element size of .03m. This study will help contribute to future work on this project. It will give future students an insight into how to perform an FEA analysis on their vehicle or on the exact vehicle used for this analysis, as well as how to perform the calculations needed to solve for the forces under any conditions they want to use.

To continue working on this project, specific changes will have to be made to improve the overall accuracy of the final results. The most noticeable change will have to be done to the geometry; the four columns will have to be taken out and redone to model a realistic ramjet interior. This process will include adding additional parts to the ramjet structure. Furthermore, fixtures and connections will be added to the structure to accurately represent how the structure is appropriately mounted to the rest of the vehicle. These changes to the geometry will have a significant impact on the results. The reason for this is because, with the current results, the weakest part of the structure is the four columns connecting the spike inlet to the rest of the vehicle. Once removed and properly mounted, a large amount of stress and strain saw in that location will no longer be there. The stress will be concentrated on the engine and vehicle connection. In addition to the physical changes needed to the model, changes to the forces experienced by the vehicle will also have to be done. Developing the forces experienced by the vehicle can be done using the Vehicle Loads program (VLOADs), developed by NASA's Marshall Space Flight Center in June 1997 by J.B Graham and P.L Luz. The program can calculate the launch vehicle's in-flight structural loads for a preliminary design. Moreover, the analysis for this report only considered two loading conditions. To thoroughly test whether the vehicle can realistically handle flight at any condition, this analysis will have to test many more loading conditions.

Additionally, this program calculates the structural loads for the upper stages and planetary transfer vehicles. It uses the launch vehicles input data, the performance data, engine thrust, aerodynamic coefficients and mass properties to deliver the axial forces, bending moments, and shear loads as a function of X-station along the vehicle's length [7]. The program is a primary design tool that allows faster analysis of structural loads for a launch vehicle, and it is an alternative to the expensive method of developing finite models for detailed load analysis. This tool will allow the user to understand better the loads for the given conditions the vehicle will experience. Lastly, changes using ANSYS will also have to be done, including improving the grid refinement study done to the model. This application will be made by creating more refined and intricate meshes to compute results better. This new study will include improving the quality of the current mesh. The current mesh uses an unstructured tetrahedral mesh, one of the most common meshes for 3-dimensional structures (3D). This mesh has some advantages, such as it is preferred for discretizing complex geometries, but it has increased computational time. To continue improving the mesh, combine different types of meshes into a hybrid mesh. Not all geometry parts can use the same type of mesh and require different mesh.

Some of the challenges faced during this analysis mainly consist of deriving the forces needed to complete the objective. As previously stated, the objective revolves around performing ramjet structural analyses using FEA with SolidWorks and ANSYS to analyze, optimize, and validate design performance parameters. Work will also need to be done to the MATLAB script to alter its parameters to achieve higher altitudes and Mach numbers. Lastly, more refinement with the grids in the grid refinement study. Overall the goal is to perform an FEA on a ramjet structure at specific parameters. These parameters will determine the force's effects on the vehicle and how the forces affect the structural integrity.

References

[1] Bansal, L., and Bharti, M. K. “Interactions Between Shockwaves and Combustion Process of Ramjet and Scramjet Engines.”, No. 4, September, 2020, pp. 1193–1197

[2] Blake, W. B., “AFRL-VA-WP-TR-1998-3009 MISSILE DATCOM.” No. 2, April 1993, 1998.

[3] Cope, H., and Office, L. “Ramjet Engines” Moscow, Russia, 1960.

[4] Demiral, E. “Conceptual Aerodynamic Design of Ramjet Missiles.” No. 6, January, 2017, pp. 10–100.

[5] Douglas, M., and Louis, A. C. “AFWAL-TR-81 -3130 DEVELOPMENT FEASIBILITY OF MISSILE DATCOM.” 1981.

[6] El-Sayed, A. F., “Fundamentals of Aircraft and Rocket Propulsion”, 2016.

[7] Fabrizo, V. “Model Development -.” [PowerPoint Slides]. Aerospace Engineering, San Jose State University. file:///D:/Progress%20Report-2020_11_23_Fabrizio_Vergine.pdf, 2020.

[8] Fry, Ronald. “A Century of Ramjet Propulsion Technology Evolution”, Journal of Propulsion and Power -. 27-58. 2020.

[9] Graham, J. B. L. “Preliminary In-Flight Loads Analysis of In-Line Launch Vehicles Using the VLOADS 1.4 Program.” No. 4, June, 1998.

[10] Heiser, W. H., Pratt, D. T., Daley, D. H. “Hypersonic Airbreathing Propulsion”. United States: American Institute of Aeronautics and Astronautics. 1994.

[11] Jang, J. H., and Ahn, S. H. “FE Modeling Methodology for Load Analysis and Preliminary Sizing of Aircraft Wing Structure.” International Journal of Aviation, Aeronautics, and Aerospace, Vol. 6, No. 2, 2019. https://doi.org/10.15394/ijaaa.2019.1301.

[12] Kwak. Transient time aeroelastic analysis for a supersonic flight vehicle with a ramjet engine. 42nd AIAA Fluid Dynamics Conference and Exhibit 2013. 2012.

[13] Mattingly, J. “Elements of Gas Turbine Propulsion”. 1996.

[14] Neill, S. M., and Pesyridis, A. “Modeling of Supersonic Combustion Systems for Sustained Hypersonic Flight.” Energies, Vol. 10, No. 11, 2017. https://doi.org/10.3390/en10111900.

[15] Newlands, R., and Heywood, M. “Rocket Vehicle Loads and Airframe Design.” Aspire Space Technical Papers, 2016, pp. 1–27.

[16] Li, C., Han, G., and Duan, C. “Study of Influential Factors of the Vibration Modal of the Rocket Equipment Bay and Structural Improvement Based on Finite Element Analysis.” International Journal of Aerospace Engineering, Vol. 2018, 2018. https://doi.org/10.1155/2018/9571979.

[17] Lintermann, A. “Computational Meshing for CFD Simulations”. 1998.

[18] Paleontology, Q. “Finite Element Analysis (FEA).” No. 4, 2012.

[19] Qu, K., and Zhang, X. “Finite Element Analysis of Propellant of Solid Rocket Motor during hip Motion.” Propulsion and Power Research, Vol. 2, No. 1, 2013, pp. 50–55. https://doi.org/10.1016/j.jppr.2012.12.002.

[20] Raffel, M., Wienke, F., and Dillmann, A. “Flying Qualities of Otto Lilienthal’s Large Biplane.” Journal of Aircraft, Vol. 58, No. 2, 2021, pp. 413–419. https://doi.org/10.2514/1.C036022.

[21] Raju, N., Pai, T. G., Verma, S. B., and Venkatakrishnan, L. "An Experimental Investigation of Turbo-Ramjet Engine Intake at Mach 4." AIAA Propulsion and Energy 2020 Forum, No. 8, February 2021, 2020, pp. 1–12. https://doi.org/10.2514/6.2020-3772.

[22] Song, E., & Song, J. Modeling of kerosene combustion under fuel-rich conditions. Advances in Mechanical Engineering. https://doi.org/10.1177/1687814017711388. 2017.

[23] Vaishakar, N. "The Future of Ramjet and Scramjet Engines in Engines Use and Results." No. 4, November, 2015, pp. 52–54.

[24] Newlands, R., and Heywood, M. "Rocket Vehicle Loads and Airframe Design." Aspire Space Technical Papers, 2016, pp. 1–27.

Appendix A. Ramjet Sizing

```
%% Ramjet Thrust Analysis
```

```
% Part A
% Inputs and Assumptions                    % Dimensions
%%%%%%%%%%%%%%%%%%%%%%%%%%%%%%%%%%%%%%%%%%%%%%
% Intial Parameters
% Velocity
V = 299.86;                                  % M/s (Intial Velocity M = 1)

% Inital Mach
M_0 = 10.16;                                 % Non Dimensional

% Intial Velocity
V_0 = 3048;                                  % M/s

% Intial Temperature
T_0 = 222;                                   % K

% Intial Total Temperature
Tt_0 = 4809.58;                              % K

% Temperature ratio at the area of the throat
T3_T0 = 7;                                   % K
%%%%%%%%%%%%%%%%%%%%%%%%%%%%%%%%%%%%%%%%%%%%%%

% General Parameters
% Fueling Ratio
f = .04                                      % Non Dimensional (Bound to 1 max)

% Enthalpy of Fuel entering the combustor
hf = 0;                                      % Energey
% Low heating value of fuel
hpr = 87806500;                              % J/kg fuel
fhpr = 3510000;                              % J/kg

% Intial specific heat at constant pressure
Cpo = 1000;                                  % J/kgK

% Specific heat at constant pressure of the combustor
Cpc = 1090;                                  % J/kgK

% Gas constant
R = 289.3;                                   % (m/2)^2/K

Vfx_V3 = 0.5;                                % Non Dimensional
Vf_V3 = 0.5;                                 % Non Dimensional
Cf_Aw_A3  = 0.1;                   % Non Dimensional

% Specific heat at constant pressure of the burner
Cpb = 1510;                        % J/kgK

% Specific heat at constant pressure of the exit
```

```
Cpe = 1510;                  % J/kgK

% Efficiencies
eta_c = 0.9;                  % Non Dimensional
eta_b = 0.9;                  % Non Dimensional
eta_e = 0.9;                  % Non Dimensional
%
P10_po = 1.4;                 % Non Dimensional

% Gravity
g_o = 9.81;                   % m/s^2

%Gammas
% Initial Gamma
gamma_o = 1.4;                % Non Dimensional
% Gamma at the combustor
gamma_c = 1.362;              % Non Dimensional
% Gamma at the exit
gamma_e = 1.238;              % Non Dimensional
% Gamma at the burner
gamma_b = 1.238;              % Non Dimensional

% Intial Pressure
po = 5582;                    % Pa

% Outputs

%%%%%%%%%%%%%%%%%%%%%%%%%%%%%%%%%%%%%%%%%%%%%%%%%%%%%%%
% Compressor components
Sao = V_0*(1 + R*T_0/V_0^2);                 % Sao
T3 = T3_T0*T_0                               % Teperature in the begining of the combustor
V3 = sqrt( V_0^2 - 2*Cpc*T_0*(T3_T0 -1));    % Velocity at the begining of the combustion chamber
M3 = V3/sqrt(gamma_c*R*T3);                  % Mach 3
Sa3 = V3*(1 + R*T3/V3^2);                    % Sa3
P3_P0 = (T3_T0/(T3_T0*(1- eta_c)+eta_c))^(Cpc/R);
P3 = P3_P0*po;                               % Pressure at the combustor
A3_A0 = T3_T0/P3_P0 * V_0/V3;                % Area at the combustor

%%%%%%%%%%%%%%%%%%%%%%%%%%%%%%%%%%%%%%%%%%%%%%%%%%%%%%%
% Combustion Component (3-4)
a = 1 - R/2/Cpb;
b = V3/(1+f)*(1+R*T3/V3^2 +f* Vfx_V3 - Cf_Aw_A3/2);
c = R*T3/(1+f)*(1+1/(Cpb*T3)*(eta_b*fhpr+f*hf+f*Cpb*T_0 +(1+f*Vf_V3^2)*V3^2/2));

V4 = V3 *((1 +f*Vfx_V3)/(1+f)-Cf_Aw_A3/(2*(1+f)))                          % m/s
T41 = T3/(1+f)*(1+1/(Cpb*T3)*(eta_b*fhpr+f*hf+f*Cpb*T_0+(1+f*Vf_V3^2)*V3^2/2))-V4^2/(2*Cpb)
% Baseline m/s
M4 = V4 / sqrt(gamma_b*R*T41);
A4_A3 = (1 + f)*T41/T3*V3/V4;

%Either Constant Pressure or Constant Area Combustion
```

```
Sa4 = V4*(1+R*T41/V4^2);

%%%%%%%%%%%%%%%%%%%%%%%%%%%%%%%%%%%%%%%%%%%%%%%%%%%%%%%%%%%%%%%%%%%
% Expanson Component (4 to 10)
p4_p0 = (1+f)*P3_P0*T41/T3*V3/V4
P4 = p4_p0*po                                      % Pa
T10 = T41 *(1-eta_e*(1-(P10_po/p4_p0)^(R/Cpe)));   % K
V10 = sqrt(V4^2 + 2*Cpe*(T41-T10));                % m/s
M10 = V10/sqrt(gamma_e*R*T10);                     % Non Dimensional
Sa10 = V10*(1+R*T10/V10^2);
A10_A0 = (1+f)/P10_po*T10/T_0*V_0/V10;             % Non Dimensional
P10 = P10_po*po;                                   % Pascals

%%%%%%%%%%%%%%%%%%%%%%%%%%%%%%%%%%%%%%%%%%%%%%%%%%%%%%%%%%%%%%%%%%%
% Engine Performance Parameters
F_m_dot_o = (1+f)*Sa10-Sao-R*T_0/V_0*(A10_A0 - 1);       % N-s/kg
S = f/F_m_dot_o;                                         % kg/s-N
eta_o = V_0/(hpr*S);                                     % Non Dimensional
ISP = hpr/g_o/V_0*eta_o;                                 % S
eta_thermal =(((1+f)*V10^2/2)-V_0^2/2)/f/hpr;            % Non Dimensional
eta_prop = eta_o/eta_thermal;                            % Non Dimensional

% Baseline
%%%%%%%%%%%%%%%%%%%%%%%%%%%%%%%%%%%%%%%%%%%%%%%%%%%%%%%%%%%%%%%%%%%
Inlet = 0;                    % Station number 0
Temp0 = T_0;                  % Station 0 Temperature (K)
Pressure0 = po;               % Station 0 Pressure (Pa)
Velocity0 = V_0;              % Station 0 Velocity (m/s)
Mach0= M_0;                   % Mach at the Inlet

Combustion_Entry = 3;         % Station number 3
Temp3 = T3;                   % Station 3 Temperature (K)
Pressure3 = P3;               % Station 3 Pressure (Pa)
Velocity3 = V3;               % Station 3 Velocity (m/s)
Mach3 = M3;                   % Mach at the Combustion Entry

Combustion_Exit = 4;          % Station number 4
Temp4 = T41;                  % Station 4 Temperature (K)
Pressure4 = P4;               % Station 4 Pressure (Pa)
Velocity4 = V4;               % Station 4 Velocity (m/s)
Mach4 = M4;                   % Mach at the Combustion Exit

Expansion = 10;               % Station number 4
Temp10 = T10;                 % Station 4 Temperature (K)
Pressure10 = P10;             % Station 4 Pressure (Pa)
Velocity10 = V10;                % Station 4 Velocity (m/s)
Mach10 = M10;                    % Mach at the Combustion Exit

Baseline_Station =[Inlet,Combustion_Entry,Combustion_Exit,Expansion];
Baseline_Mach =[Mach0,Mach3,Mach4,Mach10];
Baseline_Temp =[Temp0,Temp3,Temp4,Temp10];
```

```
Baseline_Pressure =[Pressure0,Pressure3,Pressure4,Pressure10]
Baseline_Velocity =[Velocity0,Velocity3,Velocity4,Velocity10];
```